Journal Pre-proofs

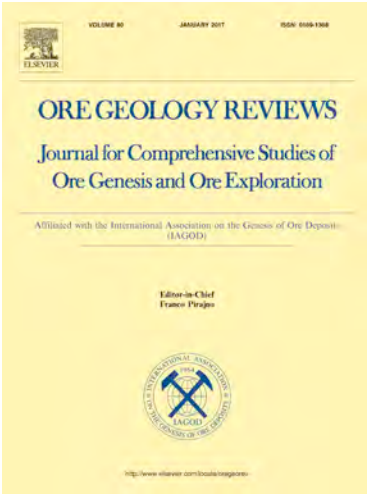


# Formation of serpentinite-hosted, Fe-rich arsenide ores at the latest stage of mineralization of the Bou-Azzer mining district (Morocco)

Zaineb Hajjar, Fernando Gervilla, Isabel Fanlo, José-María González Jiménez, Said Ilmen

PII: S0169-1368(20)31111-2
DOI: https://doi.org/10.1016/j.oregeorev.2020.103926
Reference: OREGEO 103926

To appear in: *Ore Geology Reviews*

Received Date: 24 July 2020
Revised Date: 22 October 2020
Accepted Date: 7 December 2020

Please cite this article as: Z. Hajjar, F. Gervilla, I. Fanlo, J-M. González Jiménez, S. Ilmen, Formation of serpentinite-hosted, Fe-rich arsenide ores at the latest stage of mineralization of the Bou-Azzer mining district (Morocco), *Ore Geology Reviews* (2020), doi: https://doi.org/10.1016/j.oregeorev.2020.103926

# Formation of serpentinite-hosted, Fe-rich arsenide ores at the latest stage of mineralization of the Bou-Azzer mining district (Morocco)

**Zaineb Hajjar [a*], Fernando Gervilla [a, b], Isabel Fanlo[c], José-María González Jiménez [a], Said Ilmen [d]**

[a] Departamento de Mineralogía y Petrología, Universidad de Granada, Facultad de Ciencias, Avda. Fuentenueva s/n, 18002 Granada, Spain.

[b] Instituto Andaluz de Ciencias de la Tierra (UGR-CSIC), Avda. Palmeras, 4, Armilla, 18100 Granada, Spain.

[c] Departamento de Ciencias de la Tierra, Universidad de Zaragoza, c/ Pedro Cerbuna 12 (Edificio Geológicas), 50009 Zaragoza, Spain.

[d] Greenfield Cobalt Exploration Team, Bou Azzer cobalt mine, Managem Group. Tour B, Twin center, Casablanca, Morocco.

*To be resubmitted*

*to*

*Ore Geology Reviews*

*Corresponding author: Zaineb Hajjar
Address: Departamento de Mineralogía y Petrología, Facultad de Ciencias, Universidad de Granada, Granada, Spain
Avda. Fuentenueva s/n 18002 Granada
Phone: +34 958 24 66 19
E-mail: zainebhajjar@correo.ugr.es

## Abstract

The Bou Azzer district in the central Anti-Atlas of Morocco is the world's unique mining district where Co is exploited from serpentinite-hosted hydrothermal Co-Ni-Fe arsenide ores. This paper provides the first-ever mineralogical and geochemical characterization of a suite of Fe-rich arsenide orebodies found during recent mining in the Ait Ahmane area, in central Bou Azzer district. These are lens-like orebodies of massive and disseminated Fe-rich ores fully hosted in serpentinites (hereafter named as serpentinite-hosted ores) that are typically enveloped by arsenide-poor, carbonated serpentinite, evolving irregularly outwards to talc-rich serpentinite. The central part of these orebodies mainly consists of massive ore made up of aggregates of zoned spindle-like crystals of löllingite whereas the outer zone of disseminated ore consists of rosette-like löllingite. These ores often contain accessory grains of chromite that display strong fracturation, zoning and alteration.

We propose a general model for the formation of the Bou-Azzer Co-Ni-Fe arsenide ores associated to the infiltration of high-temperature (>400ºC) slightly alkaline, oxidized and $CaCl_2$-rich fluids through opening fault and fractures. When channeled through faults separating serpentinite and quartz diorite (or other rocks) the fluids deposited Ni- and Ni-Co-rich ores in these fault-related open spaces (here re-defined contact-type ores). Over the course of mineral deposition, the generated Ni-poor fluids tended to migrate into serpentinite, first through networks of thin entwined veins and progressively by intergranular percolation, promoting dissolution of the infiltrated serpentinite and precipitation of Co-Fe ores (the presence of remnants of chromite included in coexisting arsenides and calcite sustains the role played by dissolution/precipitation, ore-forming process). Further circulation of the evolving fluids through weak zones of massive serpentinite away from the serpentinite-quartz diorite (or other rocks) contact (intra serpentinite faults), formed the serpentinite-hosted, Fe-rich ore type represented by the F55 lens. These fluids most probably evolved at low temperature (~200ºC) towards slightly higher pH values and oxidizing conditions increasing the proportions of $CO_2$ and $CO_3^{2-}$, promoting the dissolution of serpentine, the increase in the magnetite component of chromite,

the formation of Cr and Fe hydroxides, the mobilization of silica out of the reactive zone and the precipitation of calcite+Fe-rich arsenides.

**Keywords:** Fe-ores, Serpentinite hosted ores, F55 lens Ait Ahmane area, Bou Azzer district.

## 0. Introduction

Most cobalt's world production is obtained as a by-product from sediment-hosted, magmatic Ni-Cu and laterite deposits and only a small percentage (16% in 2016) is produced as a primary commodity (Alves-Dias et al., 2018). The latter production is mostly extracted from the hydrothermal deposits of the Bou Azzer mining district in Morocco where Co is beneficiated from Co-Ni-Fe arsenide ores. Although the alteration products of these ores (mainly erythrite: $Co_3(AsO_4)_2.8H_2O$) were known for a long time by the inhabitants of the Bou Azzer region who used them as insecticides and in rat poison, the history of this mining district started in 1929 when Jean Epinat, a French industrialist, was taken to the area and discovered several ore outcrops composed of complex assemblages including oxides, carbonates, arseniates and arsenides (Nataf, 2003). Afterwards, these mineralizations were exploited under artisanal mining mode, which was soon followed by the opening of the Bou Azzer mine in 1934 (Maacha et al., 2011). Since then, the Bou Azzer deposits have been an important source of Co and nowadays produce up to 2,500 tons of cobalt, 1,0000 tons of arsenic, 300 tons of nickel and 250 kg of gold (Bouabdellah, et al., 2016).

The Co-Ni-Fe arsenide ores in the Bou Azzer district are WNW-ESE flame-shaped orebodies, flat lenses and pocket-like masses located at the contacts between serpentinite bodies and quartz diorite or, locally, gabbros, younger volcanic rocks and sedimentary rocks (here after contact ores). Arsenide ores also fill NE-SW, N-S cross-cutting veins hosted in all these rocks (here after cross-cutting ores) (Leblanc, 1975; En-Naciri, 1995; El Ghorfi, 2006; Gervilla, 2012; Maacha, 2013; Bouabdellah, et al., 2016; Ikenne et al., 2020). The crystallization sequence of the mineralized bodies was summarized in three stages by Maacha, (2013) and Bouabdellah et al., (2016): (a) a pre-arsenide

ore consisting of gold associated to chlorite and quartz, (b) an arsenide stage made up of mono-, di- and tri-arsenides, and sulfarsenides, and (c) an epithermal stage marked by the precipitation of sulfides associated to late quartz and calcite. At deposit scale, contact ores tend to be rich in Ni and Ni-Co arsenides [nickeline, NiAs; rammelsbergite, $NiAs_2$; Ni-rich skutterudite $(Co,Ni)As_3$, members of the rammelsbergite ($NiAs_2$)-safflorite ($CoAs_2$), and the rammelsbergite ($NiAs_2$)-safflorite CoAs)-löllingite ($FeAs_2$) solid solution series] in the center of lodes evolving progressively to Co- and Fe-rich arsenide assemblages (mainly containing skutterrudite, members of the löllingite-safflorite series and löllingite) towards the disseminated ores found in serpentinite (Leblanc, 1975; En-Naciri, 1995; Gervilla et al., 2012). Fluid inclusions studies on pre- and post-ore quartz, and post-ore calcite show the presence of moderate to highly saline fluids (15-22 wt% NaCl and 16.5-20.5 wt% $CaCl_2$) trapped at low temperatures (120-240ºC) under variable pressures (0.4-1.2 kb) (En-Naciri, 1995). In contrast, primary inclusions in pre-ore quartz identified by Dolansky (2007) yielded information on mineralizing fluids being highly saline brines (31-42 wt% NaCl and 6-13 wt.% $CaCl_2$) that were trapped at relatively higher temperature (298-409ºC) under relatively high pressures (1.6-2.5 kb). This information obtained from fluid inclusion along with phase relations and mineral geothermometry of arsenides (Gervilla et al., 2012), seems to indicate a general trend of decreasing temperature of ore formation within single deposits with Ni-rich ores formed at higher temperatures than Co- and Fe-rich ones. Available C, O and H isotopic data (Dolansky, 2007; Maacha et al., 2015a,b) argue for the presence of both magmatic and exogenic water for the formation the arsenide ores.

Two newly-discovered ore deposits (F53 and F55) were mined by the Managem Group in the Ait Ahmane area in 2018 but since 2019, mining operations only remained active in the F53 deposit, becoming the main ore deposit in the area from the seventies of the past century. Two types of orebodies coexist in the F53 deposit: 1) massive ores found along the contact between serpentinites and quartz diorite (hereafter contact-type ores), and 2) semimassive to disseminated ores in quartz veins cross-cutting quartz diorite (hereafter, cross-cutting-type ores). These two types of ores were exploited in 2019, producing raw material with up to 2.40% Co and 0.20% Ni on average. The F55 deposit is a 95 meters-long and up to 9 meters-thick lens of massive to disseminated ores hosted by

serpentinite, having Co and Ni contents similar to those of the F53 deposit (2,03% and 0.75% respectively), which are significantly higher Co and slightly lower Ni than the average grades (~1% Co and 1% Ni) reported for the whole Bou Azzer district (Bouabdellah et al., 2016).

The different contact-type orebodies of the Bou Azzer district have traditionally been interpreted as fillings of fault-related, open spaces created along the contacts between quartz diorite intrusions (or locally gabbros, volcanic or sedimentary rocks), and serpentinites (Leblanc, 1975; En-Naciri, 1995; El Ghorfi, 2006; Maacha, 2013; Bouabdellah, et al., 2016; Ikenne et al., 2020). However, texture of the arsenide ores in the Aghbar deposit (Gervilla et al., 2012) shows replacement relationships between ores and their host serpentinite suggesting that such ores formed at expenses of serpentinite rather than by simple filling of open fractures. Thus, the identification of serpentinite-hosted orebodies (serpentinite-hosted ores) at Ait Ahmane as well as the presence of volumetrically important disseminated ores in serpentinites in the Aghbar deposit (Gervilla et al., 2012; Fanlo et al., 2015) with high Co/Ni ratios rise two important questions to understand the spatial evolution of the Bou Azzer hydrothermal system at different scales and the local mechanisms of ore formation: 1) how ore-forming fluids migrate into, and extend towards the host serpentinite? and 2) why serpentinite hosted ores are mainly made up of Co- Fe arsenides?

This paper aims to answer these two questions providing new knowledge that may help to explore new ore deposits in this worldwide unique mining district as well as to plan exploitation strategies within single deposits. In order to achieve this goal we provide a very careful updated characterization of the mineralogy and chemistry of the F55 ore lens comparing it with the nearby, already exploited F56 lens and the contact-type ores of the F53 deposit both at Ait Ahmane, as well as with literature and own data from the contact-type ores of the F7/5 orebody in the western part, and the Aghbar deposit in the central part of the Bou Azzer mining district (cross-cutting-type ores are not studied or discussed in this paper). Our results provide unprecedented insights on: 1) the mineralogical and geochemical peculiarities of serpentinite-hosted ore lenses and associated alteration halos with respect to the most frequent contact-type ores; 2) the evolution of ore-forming fluids at the district scale and within single deposits and 3) the extent of interaction between mineralizing fluids and the

host serpentinite. Whole-rock geochemical data from the F55 ore lens and its variably altered host rocks, the F56 lens, the contact-type ores of the F5/7 orebody and the Aghbar deposit will also allow discussing the possible provenance of major ore-forming elements (As, Co, Ni and Fe).

## 1. Geology

The Bou Azzer El Graara inlier is located in the western part of the central Anti-Atlas (Morocco) (Choubert, 1963; Leblanc, 1975; Saquaque et al., 1989; Figure 1) and is mainly composed of Proterozoic terranes, from early Cryogenian to late Ediacarian (D'Lemos et al., 2006; Blein et al., 2014). The oldest of these terranes is located in the southern part of the Bou Azzer inlier and includes two units: the Tachdamt Bleida unit and the Tazegzaout unit. The Tachdamt Bleida unit is composed of stromatolitic limestone, quartzite, tholeiitic basalts and schists, and represents a passive margin formed during Tonian or Early Cryogenian (Clauer, 1974; Bouougri et al., 2020). The Tazegzaout unit is composed of orthogneiss, metagabbro, schists and pegmatite attributed too to Early Cryogenian (D'Lemos et al., 2006; Blein et al., 2014; Hefferan et al., 2014). These units were previously considered Paleoproterozoic (PI) by Leblanc (1981).

The late Cryogenian terrane is represented by three units: the Tichibanine Ben Lagrad Group, the ophiolite complex and the Ousdrat suite. The first group consists of a complex tectonic assemblage made up of metagreywackes and arc-related basalts, andesites, rhyolites and tuffs (Tekiout, 1991; Naidoo et al., 1991). This volcanic arc was dated to be active between 761 ± 7 Ma and 767 ± 7 Ma (zircon U-Pb age) from a rhyolite sample by Blein et al., (2014). The ophiolite complex includes, from bottom to top, serpentinized mantle peridotites, gabbros (by zircon U-Pb age: 697 ± 8 Ma (Bodinier et al., 1984; El Hadi et al., 2010); 758.7 ± 2.1 Ma and at 659 ± 7 by apatite U-Pb age (Hodel et al., 2020)), sheeted dykes, submarine pillow basalts and locally, a varied set of partly metamorphosed sedimentary rocks, including metapelites, sandstones and limestones. The Ousdrat Suite is made up of diorite, quartz-diorite and monzodiorite intruding the ophiolite complex. These intrusions are dated at 640-670 Ma (Mrini, 1993; Inglis et al., 2003; Samson et al., 2004, Blein et al., 2014; Triantafyllou et al., 2020).

The Ediacaran terranes are also represented by three groups; the Bou Lbarod group, the Tiddiline group, and Ouarzazate group. The Bou Lbarod Group consist of mafic volcanic rocks intruded by post-kinematic stocks such as the Bleida granodiorite dated, using the U-Pb method in zircons, between 630 and 580 Ma ago (Inglis et al., 2004; Blein et al., 2014). The Tiddiline group unconformably overlies the ophiolite series and is composed of terrigenous sediments (siltstone and conglomerate) with local pyroclastic rocks (U-Pb age on zircons of 606 ± 5 Ma ; Blein et al., 2014). The Ouarzazate Group gathers a suit of potassic to high-potassic volcanic rocks (ignimbrites and tuffs) made up of andesites, dacites and rhyolites, interstratified with chaotic breccia, polygenic conglomerates and arkosic sandstones. The U-Pb age obtained on 10 zircon grains from a rhyolitic welded tuff of the Ouarzazate bracketed the time of formation of this group between 567 ± 5 Ma and 566 ± 4 Ma (Blein et al., 2014). A Lower Cambrian-Upper Proterozoic, carbonate-dominated sedimentary succession (Adoudou and Lie-de-vin formations; Choubert, 1963), dated at 541 ± 6 Ma by U-Pb on seven zircons (Blein et al., 2014), overlies the Ouarzazate group.

The Ait Ahmane area is located in the central portion of the Bou Azzer-El Graara inlier but includes the easternmost outcrops of Co-Ni arsenide ores of the Bou Azzer mining district (Figure 1). This area also includes the most complete outcrop of the lithological units that constitute the ophiolite sequence (Choubert, 1963; Leblanc, 1975, 1981; Boudinier et al., 1984; El Hadi, 1988; Saquaque, 1992; Hilal 1991; Admou, 2000; Maacha, 2013; Bhilisse, 2018). The serpentinite outcrops are usually bounded to the south by quartz diorite intrusions dated at 650 ±2 Ma using U-Pb on zircons (Inglis et al., 2003). In this area Leblanc, (1981) identified up to ten mineralized veins (from F51 to F61), many of which were mapped (1/1000) by the geological service of CTT mine of Bou Azzer (Figure 2).

Three types of ores can be distinguished in the Ait Ahmane area (En-Naciri, 1995; El Ghorfi, 2006; Talha, 2011; Hajjar, 2011; Bouchador, 2012; Maacha, 2013): 1) carbonate-bearing, ore lenses located along the contact between serpentinite and gabbro (F54, F51, F57) or quartz diorite (F53, F52) (i.e., contact-type ores). These lenses are made up of Co-Ni-Fe arsenides associated with calcite, quartz and minor talc and serpentine. They show two arsenide assemblages: an earlier, Ni-rich one composed of nickeline (rare), rammelsbergite-safflorite, rammelsbergite-safflorite-löllingite and

gersdorffite (NiAsS), intersected by a second, Co- and Fe-rich one constituted by skutterudite, löllingite-safflorite and löllingite (En-Naciri,1995; El Ghorfi, 2006; Lasobras, 2012; Maacha, 2013). 2) Quartz-calcite, arsenide ores filling cross-cutting veins within quartz diorite and gabbro (F52, F53, F54, F57) (i.e. cross-cutting-type ores). These ores present the same mineral assemblage as type 1 (En-Naciri,1995; Maacha, 2013). 3) Carbonate-bearing, Fe-Co arsenide ore lenses hosted by serpentinite (F55, F56, F58) (hereafter serpentinite-hosted ores). These lenses show alteration halos of carbonates mainly made up of calcite and minor talc and chlorite; they were not previously investigated. Types 1 and 3 are oriented WNW-ESE following the most frequent, regional orientation of arsenide orebodies in the Bou Azzer district whereas type 2 arranges almost perpendicularly (NNE-SSW).

## 2. Samples and analytical methods

This study was mainly performed on the basis of eighteen samples collected from the F55 lens and its host rocks and two samples from the F56 lens (Figure 3). The F55 lens was under exploitation in November 2016, at the time of our field campaign, allowing complete sampling along two cross sections intersecting the main lens, as well as the host, variably altered serpentinites. The F56 lens was completely exploited at that time and the few highly weathered ore remains did not provide material enough for representative sampling; thus, only one fresh sample and a partly altered one could be collected for comparison. The samples were cut, mounted on a glass plate and polished at the Department of Mineralogy and Petrology of the University of Granada (Spain) for petrographic observations. They were studied under transmitted- and reflected-light, polarized microscope, as well as by a SUPRA40VP scanning electron microscope at the Centro de Instrumentation Científica (CIC) of the University of Granada, Spain, using STEM and EDX detectors. Operating conditions were: accelerating voltage of 20 kV, beam current of 20 nA and count times of 20 s.

The chemical composition of arsenide ore minerals (Appendix A) and chromite (Appendix B) was obtained by using two different electron-probe instruments. Arsenides were analyzed in the Centros Científicos y Tecnológicos (CCiT) of the University of Barcelona (Spain) using a JEOL JXA-8230 instrument equipped with five WDS spectrometers, under an excitation voltage of 20 kV and a beam current of 20 nA, with a beam 2-3 μm in diameter. Monitored spectral lines were AsLα, SKα,

SbKα., FeKα, CoKα, NiKα, and BiLα. Pyrite, GaAs, NiO, as well as pure Co, Cu, Au, Zn, Bi and Pb metal were used as primary standards. Chromite analyses were performed at the Centro Instrumentación Científica (CIC) of the University of Granada by means of a CAMEBAX SX100 instrument under excitation voltage of 20 kV, beam current of 20 nA and beam diameter of 5 μm. Monitored spectral lines were MgKα, FeKα, AlKα, CrKα, SiKα, TiKα, MnKα, NiKα, VKα, and CoKα using MgO, $Fe_2O_3$, $Al_2O_3$, $Cr_2O_3$, $SiO_2$, $TiO_2$, $MnTiO_3$, NiO, $V_2O_3$, ZnS, NiO, and metallic cobalt as standards.

Nineteen whole-rock samples from the F55 and F56 veins and their host altered and unaltered serpentinite as well as ten arsenide ore samples from the F7/5 orebody and four from the Aghbar deposit (located, respectively, in the western and central parts of the Bou Azzer mining district) were Analyzed at INTERTEK (Australia) for S, As, Fe, Co, Ni, Os, Ir, Ru, Rh, Pt, Pd and Au. The method used to determine Cu, Fe, Ni and S concentrations involved sodium peroxide fusion followed by dilution in concentrated hydrochloric acid followed by Inductively Coupled Optical Plasma Emission Spectrometry. The analysis of As, Co, PGE and Au were performed by nickel sulfide fire assay collection prior to Inductively Coupled High Resolution Plasma Mass Spectrometry (ICP-MS). Detection limits were 20 ppm for As, Co, Cu, and Ni, 0,1wt. % for Fe, 0,05 wt. % for S, 1 ppb for PGE and 2 ppb for Au. However, arsenide ore samples with >40 wt. % As were very difficult to fuse forcing to diminish the weight of the charges down to 1 gram, what rose the detection limit of these noble metals up to 25 ppb. These analytical conditions didn't allow measuring Os, Ir and Rh from some arsenide-rich, massive ores.

## 3. The arsenide ore lenses

### 3.1. Petrography

The two deposits (F55 and F56) analyzed in this study are of the serpentinite-hosted type, fully hosted in serpentinites whose protolithic rocks were metadunite and metaharzburgite now made up of mesh-textured lizardite and antigorite with minor chrysotile (Figure 4B) as well as scattered and isolated chromite grains (200-400 μm across). Partly altered (bastitized) orthopyroxene are still preserved in harzburgitic rocks.

The F55 deposit has a flat lens shape striking N120E and dipping 62º to SW (Figure 3; Figure 4A). It shows a zoned structure consisting of a massive core (modal proportions of arsenides vary from ~60% to almost 100%) surrounded by a variably-thick (2.5-7 m) envelope of disseminated ore in carbonated serpentinites. The core-envelope transition is often gradual as well as the external limits of the envelope which evolve outwards to progressively less carbonated rocks and locally to talc-rich serpentinites. The main carbonate mineral in this halo is calcite which is found fillings irregular veinlets in serpentinite (Figure 4C and D), locally with minor talc and chlorite interstitial to calcite grains. Calcite also replaces serpentine at the veinlet walls, especially in zones characterized by tight networks of such veinlets giving rise to rocks almost completely composed of calcite. Chromite remains either in the serpentinite matrix or included in calcite where it becomes partly corroded. Talc-rich serpentinites often show fibrous texture (Figure 4E) and contain scattered small (50-100 µm across) crystals of magnetite and partly altered chromite (200-400 µm across). The latter is usually zoned showing unaltered cores surrounded by variably thick (25-50 µm) rims of ferrian chromite.

Massive arsenide ore forming the central part of the F55 lens (>70 vol.% arsenides) mainly consists of aggregates of spindle-shaped, zoned crystals of Fe-rich diarsenides (mainly löllingite) containing, serpentine, chlorite and chromite inclusions (Figure 5A, F) as well as minor nickeline, chalcopyrite and sphalerite, in a calcite matrix. Chromite grains are often fractured and also occur included in the coexisting calcite.

Likewise, the disseminated ore located in the carbonated halo also consists of löllingite, which forms rosettes and spindle-shaped grains scattered in the calcite-dominated, talc- and serpentine-bearing matrix (Figure 5B and C). Transition between massive and disseminated ores takes place through a zone of semimassive ores where Co-Fe arsenides fill thin entwined veins in a carbonated, partly mineralized serpentinite matrix. Löllingite rosettes often show Co- and at lesser extent Ni-rich growth bands or contain Ni-rich cores (Figure 6A, b and C), which include tiny grains (10-20 µm across) of native bismuth and at lesser extent galena and chalcopyrite. Chromite is also a minor constituent of this assemblage occurring as partly fractured and altered grains included in löllingite and calcite. Chromite associated to calcite in both massive and disseminated ores frequently shows

irregular alteration to a less reflective heterogeneous material, progressing along fractures and replacing the core of chromite crystals, thus giving rise to irregular, partly altered or atoll-shaped grains.

The F56 deposit is a lens with a flatter-like morphology and smaller in size (maximum thickness of 6 m and 35 m in length) than F55. It is oriented as the F55 within the serpentinite host rock although it is attached to a small intrusion of quartz diorite (Figure 3). It develops a halo of carbonated serpentinite which contains partly weathered, subhedral crystals of skutterudite (~40 mod. %) as well as rosettes and aggregates of spindle-shaped, zoned crystals of löllingite containing bands of löllingite-safflorite, both included in calcite (Figure 5D and E; Figure 6D, e and F). Arsenide minerals contain inclusions of serpentine, some chlorite and corroded grains of chromite. Sulfide minerals are also present as galena grains included in löllingite-safflorite and disseminated crystals of arsenopyrite.

### 3.2. Mineral chemistry of arsenides

The chemical composition of diarsenides from the F55 lens plots in the Ni-poor region of the $CoAs_2$-$NiAs_2$-$FeAs_2$ (safflorite-rammelsbergite-löllingite) system, most of them (~75% of spot analyses) clustered on the Fe-rich end (löllingite) of the $CoAs_2$-$FeAs_2$ binary (Figure 7A). In massive ores, spindle-shaped crystals consist of Ni-poor löllingite (<0.63 wt.% Ni) with diffuse sector zoning and/or alternate bands characterized by slight enrichments of Co (up to 3.21 wt.%) but often include bands with significantly higher Co contents (12.51-19.49 wt.% Co) (Figures 6B and Figure 7A, Appendix A). Diarsenides occurring as rosettes show Ni-richer cores with compositions plotting along the rammelsbergite-löllingite joint (6.16-12.92 wt.% Ni, 7.79-13.33 wt.% Fe and 0.47-2.26 wt.% Co) evolving outwards through narrow bands of rammelsbergite-safflorite-löllingite (6.71-8.22 wt.% Ni, 9.40-14.52 wt.% Co and 7.79-13.33 wt.% Fe) to compositions close to the löllingite corner (27.12-28.83 wt.% Fe, 0-0.11 wt.% Ni and 0.05-1.38 wt.% Co) (Figure 7A; Appendix A).

Diarsenide rosettes from the F56 lens show the same pattern of zoning of löllingite rosettes from F55, having cores slightly enriched in Ni (2.19-4.83 wt.% Ni) surrounded by rims of almost pure löllingite often containing bands enriched in up to 5.4 wt.% Co (Figure 7A). The composition of the


11

different zones and bands of spindle-shaped crystals, both disseminated and forming aggregates, extend along the löllingite-safflorite joint, from nearly pure löllingite to safflorite containing up to 1.34 wt.% Fe and 3.24 wt.% Ni.

The compositions of diarsenides from F55 and F56 ore lenses partly overlaps those reported by El Ghorfi, (2006) for the F51 lens and mainly by En-Naciri, (1995) and Lasobras, (2012) for the F53 lens, highlighting the Ni-poor and extremely Fe-rich nature of these minerals in the studied serpentinite-hosted ores.

Electron-probe micro-analyses of skutterudite reveals a diffused zoned structure with alternating Co-rich (up to 19.24 wt.% Co, 1.38 wt.% Fe and 0.62 wt.% Ni) and Ni-rich (up to 7.33 wt.% Ni, 11.66 wt.%Co and 4.7 wt.%Fe) bands. Taken as a whole, the compositional field of skutterudite from F56 ore lens partly overlaps the fields reported by Lasobras (2012) for different textural types of skutterudite from the F53 deposit but extends toward Ni-rich compositions (Figure 7B).

### 3.3. Mineral chemistry of Chromite

The studied talc-rich serpentinite sample from the outer part of the carbonated halo contains chromite with cores slightly enriched in $Fe_2O_3$ (11.44-17.96 wt.%) but with similar low Mn and Zn contents (<0.8 wt.% MnO and <0.5 wt.% ZnO) to chromite cores in noncarbonated, barren serpentinites (Figure 8). It also shows rims with higher $Fe_2O_3$ (27.13-33.74 wt.%) and slightly higher Mn (0.68-1.10 wt.% MnO) and Zn (0.23-0.70 wt.% ZnO) contents than cores (Appendix B). Chromite in carbonated serpentinite containing minor arsenides shows small core-to-rim variations in the proportion of trivalent cations both in grains associated to serpentine minerals and in those included in calcite and, as a whole, overlap the composition of chromite from the talc-rich serpentinite (Figure 8). It also shows small differences in Mn and Zn contents between grains included in calcite (0.58-0.96 wt.% and 0.24-0.47 wt.% respectively) and grains included in serpentine (0.44-0.84 wt.% MnO and 0.16-0.40 wt.% ZnO); these values are slightly lower than those of altered rims of chromite from talc-rich serpentinite. In contrast, accessory chromite in disseminated and massive ores exhibit a distinct composition mostly plotting in the Al-poor region of the Cr-$Fe^{3+}$-Al ternary (Figure 8). Although some


12

few cores of chromite grains have compositions comparable to those described from talc-rich serpentinites and poorly mineralized carbonated serpentinites ($Fe_2O_3$=10.09-16.65 wt.%, MnO=1.07-1.18 wt.%, ZnO=0.50-0.58 wt.%), the composition of most chromite grains in disseminated and massive arsenide ores (both included in calcite and in löllingite) plot in a field that overlaps and extends beyond the field of rims of highly altered chromite grains described by Gahlan and Arai, (2007) and Hodel et al., (2017), approaching the composition of magnetite (Figure 8): $Fe_2O_3$ varies from 28.00 to 65.95 wt.%, MnO from 0.28 to 3.73 wt.% and ZnO from 0.05 to 0.57 wt.%. These chromite grains do not show a general pattern of core-to-rim chemical variation but rims (where present) frequently have 1 to 2 wt.% $Fe_2O_3$ higher than cores and locally are slightly richer in Mn and Zn than cores (Appendix B). The Mn and Zn contents of accessory chromite in massive and disseminated arsenide ores of the F55 lens are comparable to those reported by Fanlo et al., (2015) from the Tamdrost arsenide ores and the F53 lens of the Aït Ahmane district, but are much smaller than the contents reported by these authors for accessory chromite from Co- and Fe-rich arsenide ores of the Aghbar deposit where MnO reaches up to 18.5 wt.% and ZnO up to 19.7 wt.%. Taken as a whole, chromite from mineralized rocks has much smaller Mg# (from 0.02-0.33) than barren serpentinite, talc-rich serpentinite and carbonated serpentinite (Mg#=0.20-0.44).

EPMA data of the less reflective material observed in some altered chromite grains showing irregular to atoll-shaped morphology (Figure 5F) reveal similar proportions of $Cr_2O_3$ and $Fe_2O_3$, with minor $Al_2O_3$, MgO, MnO and ZnO. They also contain traces of $TiO_2$, $V_2O_3$, NiO and CoO, and show low totals, ranging from 72.19 to 75.81 wt.%, thus indicating the presence of 24.19-27.81 wt.% light elements. The heterogeneous nature of this material as well as its major composition, mainly consisting of $Cr_2O_3$ and $Fe_2O_3$ with totals around 74 wt.% suggest it consists of, probably amorphous Cr and Fe hydroxides [$Cr(OH)_3$+$Fe(OH)_3$] including variable amounts of tiny chromite remains. The fact that water represents 26.18 wt.% and 25.29 wt.% of the molecular weight of $Cr(OH)_3$ and $Fe(OH)_3$ respectively, support this interpretation.


13

### 3.4. Whole rock analyses

Major ore-forming element (As, Co, Ni and Fe) contents broadly increase from serpentinite, talc-rich serpentinite and barren carbonated to partly mineralized, carbonated serpentinite and mainly in massive arsenide ores of the F55 lens (Table 1). Such enrichment trend is very clear for As and, at lesser extend Co but is poorly defined for Fe and is almost absent for Ni.

All analyzed samples (Table 1) show unusually high As contents, varying from 196.5 ppm (average) in talc-rich serpentinites to 49.03 wt.% (average) in massive arsenide ores of the F55 lens. These values are ~$10^3$ to ~$10^7$ times higher than the primitive mantle values reported by Lyubetskaya and Korenaga, (2007) (Figure 9). Co contents are quite low in barren, uncarbonated serpentinites and talc-rich serpentinites (from 13 to 169 ppm; Table 1) having primitive mantle-normalized ($Co_N$) values usually below 1 (in two samples $Co_N$ reaches 1.33 and 1.61; Figure 9). The carbonated serpentinite sample AA-6 has $Co_N$ >1 (1.26) correlated with a significant increase in As content (3.88 wt.%; Table 1). As expected, Co contents in ore samples increase up to 665 ppm Co (ave.) in disseminated ores and to 11840 ppm Co (ave.) in massive ores, representing Co enrichments 5 to 240 times the primitive mantle values (Figure 9). Ni does not show a distribution pattern comparable to that of Co since Ni contents of barren serpentinites (1050-2445 ppm) overlap those of massive arsenide ore samples (870-7093 ppm) (Table 1). As a whole, $Ni_N$ values range from slightly below 1 (down to 0.47) to slightly above 1 (up to 1.50). Only three samples surpass these values: ore samples AA-19A ($Ni_N$=2.37) and AA-20 ($Ni_N$=3.57) from the F55 lens and the sample AA-8 ($Ni_N$=2.26) from the F56 lens (Figure 9). The distribution pattern of Fe is somewhat similar to that of Ni since all barren samples but one, as well as the poorly mineralized samples from the western end of the F55 vein show $Fe_N$ values below 1 (Figure 9), corresponding to Fe contents ranging from 2.18 to 6.14 wt.% (Table 1); only the sample AA-27 has 6.57 wt.% and $Fe_N$=1.06. Ore samples are significantly enriched in Fe (from 14.05 to 22.56 wt.%; 19.98 wt.% on average) representing primitive mantle-normalized values between 2.26 and 3.63. S does not correlate with any of the other elements.

The analyzed samples from the F7/5 and Aghbar contact-type deposits have lower As (38.94% As and 38.49% As on average, respectively) and Fe (12.63 wt.% Fe and 2.21 wt.% Fe on average,

respectively) contents, but are much richer in Co (35524 ppm Co and 84125 ppm Co on average) and Ni (5533 ppm Ni and 11022 ppm Ni on average, respectively) than those from the F55 lens. These data question the suggested west to east enrichment in Ni and Fe suggested by En-Naciri (1995) because the Co- and Ni-richest ore is that from Aghbar, located in the center of the Bou Azzer district.

Whole-rock Co contents in the F55 lens are poorly correlated with those of As, which in turn shows a good positive correlation with Fe (Figures 10A and C). Ni and As are uncorrelated (Figure 10B). However, the comparison of these data with those of arsenide ores from the F56 lens, the F7/5 orebody and the Aghbar deposit split the plotted results in two well differentiated groups (Figures 10D, E and F): a group with a Co-Ni trend and a group with a Fe trend. The Co-Ni trend includes the samples from Aghbar and some from F7/5 and is defined by a positive correlation between Co and Ni with As, but Fe contents unrelated with those of As. In contrast, the Fe trend is mainly defined by the samples from F55 and most but two samples (the Co and Ni richest ones) from F7/5 and shows a good correlation between Fe and As but no correlation of Co and Ni with As. The only sample analyzed from F56 could be ascribed both to the Ni-Co trend and the Fe trend (Figures 10D, E and F).

Platinum-group element contents in barren, noncarbonated serpentinites vary from 22 to 42 ppb (Table 1) and their most frequent chondrite-normalized pattern shows a nearly flat segment from Os to Ru around $10^{-2}$ times the chondritic values (Naldrett and Duke, 1980) followed by a negative slope from Ru to Rh and a positive-sloped, variably-tilted segment from Rh to Pd (Figure 11A). Some few samples show either Ru and Pt positive anomalies or Pd negative anomalies. The talc-rich serpentinite is extremely depleted in PGE but one of the samples (AA-2) shows a significant enrichment in Pd (17 ppb). In contrast, the chondrite-normalized PGE pattern of carbonated serpentinite mostly mimic that of serpentinites. In ore samples from F55 and F56, bulk Ru, Pt and Pd contents increase above 10 times the chondritic values, as the proportion of arsenide minerals increases always showing chondrite-normalized PGE patterns with positive slopes from Ru to Pd (note that Rh could not be analyzed), plotting within the field of Co-rich ores, above that of Fe-rich ores, as defined by Leblanc and Fischer, (1990) (Figure 11B). PGE values of the F55 ores overlap those of the F5/7 orebody and the Aghbar deposit, showing comparable morphologies of their chondrite-

normalized patterns (Figure 11) but plot 10 times above the values reported by Ahmed et al., (2009a) which mostly overlap the field of barren serpentinites.

Taken as a whole, gold contents increase from barren, noncarbonated serpentinites (3-5 ppb Au) to massive ores (34-4766 ppb Au) although in some few samples (both mineralized and barren) they are below detection limit (Table 1). In spite of this trend, gold contents show no correlation with As, excepting for the four samples from the Aghbar deposit. Most samples show positive-sloped segments from Pd to Au in the chondrite-normalized patterns (Figure 11) and as expected, Au contents tend to increase from the F55 lens (99-491 ppm Au) to the F5/7 (0-2197 ppm Au) and mainly the Aghbar (225-4766 ppm Au) deposits as the relative abundance of the high-temperature, Ni-rich ores does (native Au mainly occur included in early formed nickelite and rammelsbergite; Ahmed et al., 2009b; Gervilla et al., 2012).

## 4. Discussion

### 4.1. Serpentinite-hosted versus contact ores at Bou Azzer

The studied F55 lens shows some mineralogical and structural features somehow characteristic of serpentinite-hosted ores in the Bou Azzer mining district. The most striking one is the mineralogical composition of the arsenide ore assemblage which is mainly composed of nearly stoichiometric löllingite arranged in aggregates of zoned spindle-like crystals or rosettes. The latter aggregates often contain thin growth bands composed of intermediate members of the rammelsbergite-safflorite-löllingite, rammelsbergite-löllingite and löllingite-safflorite solid solution series (Figure 6; Figure 7A). The mineral chemistry of this assemblage as a whole reveals its characteristic low Ni and relatively low Co nature, allowing a definition for this type of ores as Fe-rich. The second characteristic feature of the F55 serpentinite-hosted orebody is its zoned structure (Figure 3) consisting of massive arsenide ore enveloped by disseminated ore hosted by carbonated serpentinites (Figure 12 A).

The comparison of these mineralogical and structural features with those of the other orebodies of the Ait Ahmane district reveals that F56 (a serpentinite-hosted lens but close to a small stock of quartz-diorite) has a similar envelope of carbonated serpentinite (Figure 3), although its


16

mineralogical assemblage is not only dominated by löllingite but contains up to 40 mod. % skutterudite (Co-Fe ore). In other deposits (F1 and F53) of the Bou Azzer district, this Co-Fe ore assemblage is preceded by an earlier Ni-rich one (Ni-Co ore), mainly composed of variable proportions of nickeline, rammelsbergite-safflorite, rammelsbergite-safflorite-löllingite and skutterudite (En-Naciri,1995; En-Naciri et al., 1997; El Ghorfi, 2006, Lasobras, 2012; Maacha, 2013). Interestingly, Gervilla et al., (2012) reported a similar two-stage deposition at Aghbar where the early crystallization of Ni-rich arsenide ores was overlapped (and partly replaced) by a later event of ore formation characterized by the development of Co-Fe arsenide ores disseminated in serpentinite (Figure 12B). Furthermore, results on old samples collected by M. Leblanc for his Ph.D. Thesis from the F7/5 orebody show a similar depositional sequence characterized by an early stage of nickeline partly replaced by Ni-rich skutterudite (up to 17 wt.% Ni) followed by the crystallization of diarsenides (rammelsbergite-safflorite, rammelsbergite-safflorite-löllingite and löllingite-safflorite) (Ni-Co ore) and ending with the formation of members of the gersdorffite-cobaltite series (Fanlo et al., 2017). Nevertheless, some samples collected recently from an area currently being mined at the F7/5 orebody (their major ore-forming elements and noble metals contents are listed in Table 1) mainly consist of löllingite-dominated, arsenide ore assemblages (Co-Fe ore) disseminated in serpentine, locally with skutterudite and remnants of Ni-Co arsenides in the massive samples. These sequences of ore-forming events agree with the sequence of deposition for arsenide minerals proposed by Leblanc, (1975) and with those suggested by En-Naciri, (1995); En-Naciri et al., (1997) and Ahmed et al., (2009b) for the whole Bou Azzer district. Therefore, it can be concluded that formation of arsenide ores at Bou Azzer started with the crystallization of massive Ni arsenides followed by Ni-Co arsenides (and sulfarsenides), both filling veins mainly along the quartz diorite-serpentinite contacts, but evolved to the subsequent crystallization of Co-Fe and Fe arsenides disseminated in serpentinite, which show increasing Fe/Co ratio with increasing the distance from the contact with the quartz diorite intrusion. Thus, the ores studied in the F55 lens would represent the crystallization products of residual fluids, formed at the end of the mineralizing events of the Ait Ahmane district.

Whole-rock As, Co, Ni and Fe contents further confirm the existence of two groups of arsenide ores since massive ores from Aghbar and F7/5 deposits show high Ni and Co contents positively correlated with As (the Ni-Co trend). In contrast, massive ores from F55 and those occurring disseminated in serpentinite both in the carbonated halo of F55 and in the new samples from the F7/5 orebody are rich in Fe positively correlated with As (the Fe trend) (Figure 10).

Unlike the relatively homogeneous carbonated nature of the hydrothermal alteration halo around the F55 and F56 lenses, the alteration patterns of all other deposits vary with the lithology of the host rock. The wideness of alteration halos in contact ores from the whole Bou Azzer district ranges from centimeter- to meter-scale consisting of intense chloritization (locally with epidote), silicification and less commonly carbonatization in quartz-diorite, and of carbonatization (mainly calcite) with variable but minor chlorite and talc in the serpentinite (Leblanc, 1975; En-Naciri, 1995; Dolansky, 2007; Maacha, 2013). Ignimbrites from Aghbar become altered to chlorite and various clay mineral assemblages and carbonatization mainly forms dolomite (Dolansky, 2007). This zoning pattern of alteration halos allow correlate the deposition of Ni-rich and Ni-Co, vein-type arsenide ores with the early silicification and chloritization event [e.g. gold occurs associated to chlorite and quartz (Maacha, 2013; Bouabdellah et al., 2016) and mainly included in nickeline and rammelsbergite (Ahmed et al., 2009b; Gervilla et al., 2012)]. With the progressive decrease of pressure and temperature, the mineralizing fluids became less saline but with higher $CaCl_2$/NaCl ratio (Dolansky, 2007) giving rise to the development of the Co-Fe and later Fe arsenide ores associated with calcite alteration in serpentinites. Although fluid inclusion data are scarce and rather controversial (see En-Naciri, 1995; En-Naciri et al., 1997; Dolansky, 2007), the results obtained by Dolansky, (2007) partially agree with the conclusions obtained by Gervilla et al., (2012) from phase relations in the sense that temperature should decrease over the course of ore mineral deposition from >400ºC to >200ºC (these values correspond to trapping temperatures and represent minimum crystallization values; Dolansky, 2007). Unpublished data on chlorite geothermometry obtained from chlorite crystals associated to calcite in Co-Fe ores disseminated in serpentinites in the F7/5 orebody yielded temperatures between 187º and 269ºC (Ares, 2018). These data support the proposed timing of ore

formation and carbonate alteration in the F55 lens, at the end of the Co-Ni-Fe arsenide mineralization process, at low temperature.

### 4.2. Mechanisms of ore formation: vein filling versus replacement

The presence of inclusions of serpentine, chlorite and partly corroded crystals and fragments of fractured chromite in arsenide minerals of the F55 lens and in the mineralized serpentinites of the F53, F7/5, Aghbar and Tamdrost contact-type deposits (Gervilla et al., 2012; Fanlo et al., 2015; Ares, 2018) show that formation of Co-Fe and Fe ores in serpentinites should take place by dissolution/precipitation processes which gave rise to the replacement of serpentinite by skutterudite, löllingite-safflorite and löllingite with variable amounts of calcite. The degree of replacement should be maximum near the main zone of supply of ore-forming fluids (usually the quartz diorite-serpentinite contact) becoming progressively less important away from such zone. Since chromite is ubiquitous in serpentinites and exhibits low solubility under most geological conditions (Oze et al., 2007), it can be used as indicator of the degree of serpentinite replacement (chromite is a high-temperature magmatic mineral and cannot be formed by hydrothermal ore-forming fluids). Thus, chromite relicts shouldn't be expected in massive, Ni-rich arsenide ores but are frequently abundant in mineralized serpentinites with ~10 to 50 mod. % arsenides as occur in Aghbar, Tamdrost and the F53 orebody in Ait Ahmane (Gervilla et al., 2012; Fanlo et al., 2015). In the latter ores, the chemical composition of chromite is not modified during ore-forming processes (except for some slight Co enrichments) preserving a zoning pattern originated during early sea-floor serpentinization and/or Pan-African orogenesis (Fanlo et al., 2015). In contrast, the chromite grains studied in the F55 lens as well as those from some recent samples of the F7/5 orebody (Ares, 2018) show compositions depleted in Al and enriched in both $Fe^{2+}$ and $Fe^{3+}$, evolving towards the composition of magnetite, and locally become highly altered up to the formation of Cr and Fe hydroxides (Figure 8). This strong alteration degree of chromite took place during the mineralization process and could be associated with small changes in pH and redox conditions of the mineralizing fluids. Although the nature of ore-forming fluids is not well constrained, Dolansky, (2007) argue that they should be slightly acid (pH ~5) and reduced ($CH_4$ and $N_2$ predominate over $CO_2$ in the vapor phase and $H_2S$ in solution) containing $Cl^-$ and $HCO_3^-$ (Figure 12). Assuming that the F55 lens formed at low temperature (~200ºC), from the latest

mineralizing fluids in the Ait Ahmane district it would be possible that fluids evolved towards slightly higher pH values and oxidizing conditions, increasing the proportions of CO2 and $CO_3^{2-}$ (over $HCO_3^-$), promoting the dissolution of serpentine, the increase in the magnetite component of chromite, the formation of Cr and Fe hydroxides at $fO_2$ maxima, the mobilization of silica out of the reactive zone (Ulrich et al., 2014) and the precipitation of calcite-rich Fe arsenides. The mobilization out of silica can control the local formation of talc-rich serpentinites.

The zoned structure of the F55 lens suggest that the core of massive ore could represent the reactive zone with higher fluid/rock ratio and that the disseminated envelope should generate under decreasing fluid/rock ratios forming dense networks of thin stockwork-ore veins in a poorly disseminated serpentine matrix near the contact with the massive core, evolving outwards to less and less volume of veins up to the formation of vein-free, disseminated ores in serpentine (Figure 12A). This model could also apply to the more frequent contact ore bodies in Bou Azzer. In this scenario, it could be expected that massive Ni-Co arsenide ores form first at high temperature, filling fault-related, open spaces generated along the contacts between serpentinite and quartz diorite (gabbros, volcanic or sedimentary rocks) (Figure 12B). This type of ore should exhibit sharp contacts with the quartz diorite intrusion such as observed in F7/5. Upon the events of mineral deposition, evolving fluids were very likely first channeled along the contact between the early formed Ni-Co ores promoting their partial replacement and subsequently flooded over the serpentinite giving rise to the development of semimassive and disseminated Co-Fe ores (Figure 12B).

### 4.3. Sources for major ore-forming metals

Regardless of the magmatic or meteoric origin (or a mixture of both provenances) of the ore-forming fluids, there is a general consensus on the role played by serpentinites as source of Co and Ni; in contrast, the origin of As remains controversial (see Leblanc, 1975; Leblanc and Billaud, 1982; Leblanc and Fischer, 1990; En-Naciri, 1995; En-Naciri et al., 1997; Dolansky, 2007; Ahmed et al., 2009b; Maacha, 2013; and Bouabdellah et al., 2017). Although the whole-rock data presented here (Table 1) are still scarce, they provide valuable information on barren, variably carbonated serpentinites (from noncarbonated to serpentinites almost completely replaced by carbonates) as well

as on four deposits containing Ni-Co ores (Aghbar), Co-Fe ores (F7/5 and F56) and Fe ores (F55), thus allowing debate on the possible fluid-mediated exchange of As, Co, Ni and Fe between serpentinite and ores.

The high As content of serpentinites (up to 644 ppm) in the Ait Ahmane area (Table 1) indeed suggest a role of this rock type as source for this element. However, the extremely high As concentrations of the hosted arsenide ores of its nearby F55 lens (~$10^3$ times higher) should require extensive leaching of these serpentinites. In contrast, the analyzed samples are far to be depleted in As but still contain ~$10^4$ times the primitive mantle values (Figure 8). These values are also higher than those of other As-rich serpentinites described in literature (e.g. 6-275 ppm As, Hattori et al., 2005).

A different scenario can be envisaged for Co, Ni and Fe if one assumes that their budget in peridotites shouldn't be substantially affected by serpentinization. The contents of Co in six of the eight barren serpentinites and talc-rich serpentinites analyzed ranges from 13 to 97 ppm (Table 1), well below the values expected for serpentinites derived from depleted mantle peridotites [e.g. Marchesi et al., (2016) reports ~142 ppm Co in harzburgite and ~152 ppm Co in dunite]. Similarly, five of the eight barren serpentinites and talc-rich serpentinites, as well as the carbonated serpentinite, are depleted in Ni (931-1814 ppm Ni; Table 1) with respect to mantle harzburgite (~2106 ppm Ni) and dunite (~2905 ppm Ni) (Marchesi et al., 2016). The Fe-depleted nature of the studied Ait Ahmane serpentinites relative to the expected harzburgite and dunite protoliths is not so evident as for Co and Ni since only two of the six serpentinites, as well as the talc-rich serpentinites and the carbonated serpentinite have Fe contents (2.18-3.51 wt.%) well below those expected in dunite and harzburgite [4.77 and 5.46 wt.% Fe; calculated from Marchesi et al., (2016)]. Nevertheless, the presence of magnetite veins with bleached serpentinite walls (Hodel et al., 2017) evidence that Fe was extensively mobilized during hydrothermal alteration of serpentinites.

PGE contents in arsenide ores are 10 times above those reported for serpentinites but the morphology of the chondrite-normalized PGE patterns of the latter rocks, similar to depleted-mantle rocks but with Pd positive anomalies, suggest a more complex process of leaching. PGE leaching from serpentinites could be associated with silica alteration since the lowest values were found in the talc-


21

rich serpentinites. Au contents are anomalously high in all analyzed rock-types; in fact, serpentinites show Au values slightly above 3 to 5 times the primitive mantle values (0.88 ppb Au; Lyubetskaya and Korenaga, 2007), in spite of the depleted nature of the mantle protoliths.

The reported contents of major ore-forming elements and noble metals allow linking the origin of Co, Ni, Fe and PGE with the Bou Azzer serpentinite but do not support any connection between As and Au with such rocks. The infiltration of high-temperature hydrothermal fluids (most probably well above 400ºC) though serpentinites during the Hercynian orogeny [most geological and geochronological data support that the mineralization event took place between 380 and 310 Ma; e.g. Levresse, 2001; Gasquet et al., 2005; Dolansky, 2007; Oberthür et al., 2009; Bouahdellah et al., 2016)] leached Co, Ni, Fe and PGE from these ultramafic rocks and became channeled mainly along the quartz-diorite-serpentinite contacts promoting the crystallization of Ni and Ni-Co ores under extremely high fluid/rock ratios. The resulting Ni-impoverished fluids shifted their flow paths to the contacts between the early formed Ni-Co ores and serpentinites maintaining high fluid/rock ratios nearby the contacts but diminishing such rations away from them. With the evolution of the hydrothermal system towards lower pressures and temperatures, fluids should have precipitated those Co-Fe ores that now are partly replacing Ni-Co ores, filling thin entwined veins and/or disseminated in serpentinite. Under the lower temperature estimated (~200ºC) for the formation of the F55 lens, the residual fluids could locally concentrate along weak zones (e.g. faults) within serpentinites forming Fe ores. This mechanism of fractionation of the infiltrating (metasomatic) fluids partly explains the anomalously high Co/Ni ratio of arsenide ores relative to the same ratio in serpentinites, although more precise mass balance calculations would be necessary to assure that serpentinites are the only source of Co. Since the origin of As and Au seems unrelated with the serpentinites, they should be supplied to the mineralizing hydrothermal fluids after leaching country-rocks from older geological units. The latter may include organic-rich black shales of the Imiter Group, which could be good candidates as source of As and as additional source of Co (they contain up to 6180 ppm As and 36,8 ppm Co on average; Pasava, 1994), thus justifying the anomalously high concentration of Co (and the high Co/Ni ratio) in the Bou Azzer ores well above that expected from lixiviation of only


22

serpentinites. The origin of Au is more enigmatic but could be linked with some of the acid/intermediate igneous rocks (granodiorite, monzonite, pegmatite…) of Lower Cryogenian age present in the Bou Azzer inlier. This is clearly a fertile field for further investigation.

## 5. Conclusions

Fe-rich, serpentinite-hosted ores in the Ait Ahmane area (e.g. the F55 lens) show lens-like morphology and a zoned structure with core of massive ore evolving progressively to disseminated ore in carbonated serpentinite, arsenide-poor, carbonated serpentinite, and talc-rich serpentinite, away from the ore lens. Ore assemblage consists of löllingite in calcite-dominated gangue (± serpentine ± chlorite) containing scattered zoned grains or fragments of fractured grains of chromite. Löllingite occurs as massive aggregates of spindle-shaped, zoned crystal containing Co-rich bands or arranged in rosette-like aggregates, showing Ni-rich cores and Co- and Ni-rich growth bands. The F56 lens, occurring close to a quartz-diorite intrusion are also mainly made up of loelllingite but contain around 40 mod. % skutterudite in the arsenide ore assemblage.

In contrast to the Fe-rich, serpentinite-hosted ores, the more frequent contact-type ores in the Bou Azzer district consist of Ni-rich ores (mainly nickeline and rammelsbergite) evolving to, and partly replaced by Ni-Co (rammelsbergite-saffloritea, rammelsbergite-safflorite-löllingite, skutterrudite and safflorite) and Co-Fe ores (rammelsbergite-safflorite-löllingite, löllingite-safflorite, skutterudite, löllingite and cobaltite). Whereas Ni and Ni-Co ores tend to be massive and locate along the fault-zone that put together serpentinites and other rocks (quartz diorite, gabbros, volcanic rocks, sedimentary rocks), Co-Fe ores are preferentially found as disseminations in serpentinites. Whole-rock, major element contents further contribute to differentiate contact-type and serpentinite-hosted ores since the former show characteristic positive correlation between Ni and Co with As, whereas in the serpentinite-hosted ores As correlates only with Fe.

Accessory chromite associates only with Co-Fe- and Fe-rich ores, occurring as partly dissolved zoned grains and fragments of fractured grains included in arsenide minerals, calcite and serpentine. Its composition reveals increasing depletion in Al and Cr coupled with enrichment in $Fe^{3+}$ and $Fe^{2+}$ up to the formation of $Fe^{3+}$ and Cr hydroxides from barren carbonated serpentinites to

massive ores. These textural and chemical features support a genetic model of Co-Fe- and Fe-rich ores based on dissolution/precipitation reactions of low-temperature, ore-forming fluids while migrate through serpentinite under slightly alkaline and oxidizing conditions, with increasing $CaCl_2$/NaCl ratio. In this scenario, partly fractured and altered chromite grains constitute residues of the serpentinite replacement.

The studied serpentinite-hosted ores formed by the infiltration of low-temperature (~200ºC) hydrothermal fluids in serpentinites at the end of the Hercynian orogeny. Ore-forming fluids channeled along intra serpentinite fault zones, promoting the formation of massive ores under high fluid/rock ratio, and subsequently infiltrated into the host serpentinite through a network of thin entwined veins and intergranularly, giving rise to semimassive and disseminated ores. This model can be applied too, to the formation of contact-type ores where high-temperature fluids channeled along the fault separating serpentinite and quartz diorite (or other rocks) promoting the sequential crystallization of Ni- and Ni-Co-rich ores in fault-related open spaces followed by Co-Fe ores in serpentinites under progressively less temperature (from >400º to <200ºC). The formation of the latter ores in serpentinites took place by the same dissolution/precipitation processes as described for serpentinite-hosted ores.

Whole-rock data suggest that Ni, Co, Fe and platinum-group elements were leached out from serpentinites by the ore-forming fluids whereas As and Au should come from different lithological units in the Bou Azzer inlier. A good candidate for As could be the organic-rich black shales of the Imiter Group which could also supply additional Co. The source of Au could be related with the Lower Cryogenian acid/intermediate magmatism reported in Bou Azzer.

## 6. Acknowledgements

This research was supported by the Spanish project RTI2018-099157-A-I00 granted by the "Ministerio de Ciencia, Innovación y Universidades" as well as the Ramón y Cajal Fellowship RYC-2015-17596 granted to JMGJ by the "Ministerio de Economía y Competitividad" (MINECO). We wish thank Dr. Moha Ikenne and Dr. Ilya Prokopyev for their constructive review, which helped to improve the presentation of the data and the discussion.


24

## 7. Appendix

**Appendix A: Chemical composition of arsenide**

**Appendix B: Chemical composition of chromite**

## 8. References

Admou, H., 2000. Structuration de la paléosuture ophiolitique panafricaine de Bou Azzer-Siroua. Anti-Atlas central, Maroc. PhD thesis, Cadi Ayyad University, Marrakech, Morocco, 201p.

Ahmed, A.H., Arai, S., Abdel-Aziz, Y.M., Rahimi, A., 2005. Spinel composition as a petrogenetic indicator of the mantle section in the Neoproterozoic Bou Azzer ophiolite, Anti-Atlas, Morocco. Precamb. Res. 138, 225–234.

Ahmed, A.H., Arai, S., Abdel-Aziz, Y.M., Ikenne, M., Rahimi, A., 2009a. Platinum-group elements distribution and spinel composition in podiform chromitites and associated rocks from the upper mantle section of the Neoproterozoic Bou Azzer ophiolite, Anti-Atlas, Morocco. J. Afr. Earth Sci. 55, 92–104.

Ahmed, A.H., Arai, S., Ikenne, M., 2009b. Mineralogy and Paragenesis of the Co-Ni Arsenide Ores of Bou Azzer, Anti-Atlas, Morocco. Econ Geol, 104, 249–266.

Alves-Dias, P., Blagoeva, D., Pavel, C., Arvanitidis, N., 2018. Cobalt: demand-supply balances in the transition to electric mobility. JRC Science for Policy Report. European Commision.https://publications.jrc.ec.europa.eu/repository/bitstream/JRC112285/jrc112285_cobalt.pdf

Ares A., 2018. Las espinelas cromíferas del filón 7/5 del distrito minero de Bou Azzer (Marruecos): residuos del reemplazamiento de serpentinitas. TFM. Universidad de Huelva-Universidad Internacional de Andalucía. 54p.

Bhlisse, M., 2018. Etude structurale, minéralogique et géochimique des serpentinites associées aux minéralisations polymétalliques du district de Bou Azzer-El Graara (Anti-Atlas central). Ph.D. thesis, Cadi Ayyad University, Marrakech, Morocco, 274p.

Blein, O., Baudin, T., Chèvremont, P., Soulaimani, A., Admou, H., Gasquet, P., Cocherie, A., Egal, E., Youbi, N., Rzin, P., Bouabdelli, M., Gombert, P., 2014. Geochronological

676 constraints on the polycyclic magmatism in the Bou Azzer-El Graara inlier (Central
677 Anti-Atlas Morocco). J. Afr. Earth Sci. 99, 287–306.

678 Bouabdellah, M., Maacha, L., Levresse, G., Saddiqi, O., 2016. The Bou Azzer Co–Ni–Fe–As
679 (– Au – Ag) District of Central Anti-Atlas (Morocco): A Long-Lived Late Hercynian to
680 Triassic Magmatic-Hydrothermal to Low-Sulphidation Epithermal System, Mineral
681 Deposits of North Africa, (eds.), Mineral Deposits of North Africa, Mineral Resource
682 Reviews, 229-247

683 Bodinier, J. L., Dupuy, C., Dostal, J., 1984. Geochemistry of Precambrian ophiolites from
684 Bou Azzer, Morocco. Contrib. Mineral. Petrol., 87, 43-50

685 Bouchador, A., 2012. Etude géologique et métallogénique des gîtes arséniés de Co-Ni dans le
686 filon 57 ; Champs filonien d'Aït Ahmane, District minier de Bou Azzer, ophiolite de
687 Bou Azzer, Anti Atlas Central, Maroc. Master, Cadi Ayyad University, Marrakech,
688 Morocco, 102p.

689 Bouougri, E., Ait Lahna, A., Tassinari, C.C.G., Basei, M. A.S., Youbi, N., Admou, H.,
690 Saquaque, A., Boumehdi, A., Maacha, L., 2020. Time constraints on early Tonian
691 Rifting and Cryogenian Arc terrane-continent convergence along the northern margin of
692 the West African craton: Insights from SHRIMP and LA-ICP-MS zircon geochronology
693 in the Pan-African Anti-Atlas belt (Morocco). Gondwana Res. 85, 169-188

694 Choubert, G., 1963. Histoire géologique du précambrien de l'Anti-Atlas. Notes et mém. Serv.
695 Géol. Maroc, 162, 352p

696 Clauer, N., 1974. Utilisation de la méthode Rb–Sr pour la datation d'une schistosité de
697 sédiments peu métamorphisés : application au Pré - cambrien II de la boutonnière de
698 Bou–Azzer–El Graara (Anti-Atlas, Maroc). Earth Planet. Sci. Lett. 22, 404–412.

699 D'Lemos, R.S., Inglis, J.D., Samson, S.D., 2006. A newly discovered orogenic event in
700 Morocco: Neoproterozoic ages for supposed Eburnean basement of the Bou Azzer
701 inlier, Anti-Atlas Mountains. Precamb. Res. 147, 65–78.

702 Dolansky, LM., 2007. Controls on the genesis of hydrothermal cobalt mineralization: insights
703 from the mineralogy and geochemistry of the Bou Azzer deposits, Morocco. Master,
704 McGill University, Montréal, Canada, 162p

705 EL Ghorfi, M., 2006. Etude géochimique et métallogenique des métaux précieux (or, argent et
706 platinoïdes) associes aux minéralisations à Co, Ni, Cr de Bou Azzer-El Graara, et dans

la série de Bleida Far West, Anti-Atlas, Maroc. PhD thesis, Cadi Ayyad University, Marrakech, Morocco, 256 p.

El Hadi, H.F., 1988. Etude pétrographique et géochimique des cumulats ultramafiques et mafiques du complexe ophiolitique de Bou Azzer El Graara (Anti-Atlas, Maroc). Thèse 3ème cycle, Cadi Ayyad University, Marrakech, Morocco, 173p.

EL Hadi, H.E., Simancas, J.F., Martinez-Poyatos, D., Azor, A., Tahiri, A., Montero, P., Bea, C.M., Gonzalez-lodeiro, F., 2010. Structural and geochronological constraints on the evolution of the Bou Azzer Neoproterozoic ophiolite (Anti-Atlas, Morocco). Precamb. Res. 182, 1–14.

En-Naciri, A., 1995. Contribution à l'étude du district à Co. As (Ni, Au, Ag) de Bou Azzer. Anti- Atlas (Maroc) Données minéralogiques et géochimiques. PhD thesis, Université d'Orléans. France 245 p.

En-Naciri, A., Barbanson, L., Touray, J.C., 1997. Brine inclusions from the Co-As (Au) Bou Azzer district, Anti-Atlas, Morocco. Econ Geol, 92, 360-367.

Fanlo, I., Gervilla, F., Colás, V., Subías, I., 2015. Zn-, Mn- and Co-rich chromian spinels from the Bou-Azzer mining district (Morocco): Constraints on their relationship with the mineralizing process. Ore Geol. Rev. 71, 82–98.

Fanlo, I., Arranz, E., Subías, I., Gervilla, F., 2017. The Filon 7/5 (Bou Azzer district, Morocco): an example of Co-Ni ores formation under disequilibrium conditions. In: Mineral Resources to Discover. Proceedings of the 14th Biennial SGA Meeting, v. 1, pp. 1531-1534.

Gahlan, H., Arai, S., 2007. Genesis of peculiarly zoned Co, Zn and Mn-rich chromian spinel in serpentinite of Bou Azzer ophiolite, Anti Atlas, Morocco. J. Miner. Petrol. Sci, 102, 69-85.

Gasquet, D., Levresse, G., Cheilletz, A., Azizi-Samir, M.R., Mouttaqi, A., 2005. Contribution to a geodynamic reconstruction of the Anti-Atlas (Morocco) during Pan-African times with the emphasis on inversion tectonics and metallogenic activity at the Precambrian-Cambrian transition. Precamb. Res.140, 157–182.

Gervilla, F., Fanlo, I., Colás, V., Subías, I., 2012. Mineral compositions and phase relations of Ni–Co–Fe arsenide ores from the Aghbar mine, Bou Azzer, Morocco. Can. Mineral. 50, 2, 447–470.


27

738 Hajjar, Z. 2011. Contribution à l'étude des Filons F53, F54, F55, champs minier d'Aït
739 Ahmane (Bou Azzer, Anti Atlas, Maroc). Master, Cadi Ayyad University, Marrakech,
740 Morocco, 105p.

741 Hattori, K., Takahashi, Y., Guillot, S., Johanson, B., 2005. Occurrence of arsenic (V) in
742 forearc mantle serpentinites based on X-ray absorption spectroscopy study. Geochim.
743 Cosmochim. Acta, 69, 23, 5585–5596.

744 Hefferan, K., Soulaimani, A., Samson, S.D., Admou, H., Inglis, J., Saquaque, A., Chaib, L.,
745 Heywood, N., 2014. A reconsideration of Pan African orogenic cycle in the Anti-Atlas
746 Mountains, Morocco. J. Afr. Earth Sc. 98, 34-46

747 Hilal, R., 1991. L'ophiolite de Bou Azzer (Anti-Atlas, Maroc) structure, perographie,
748 géochimie, et contexte de mise en place. Thèse 3ème cycle, Cadi Ayyad university,
749 Marrakech, Morocco, 175p

750 Hodel, F., Macouin, M., Triantafyllou, A., Carlut, J., Berger, J., Rousse, S., Ennih, N.,
751 Trindade, R.I.F., 2017. Unusual massive magnetite veins and highly altered Cr-spinels
752 as relics of a Clrich acidic hydrothermal event in Neoproterozoic serpentinites (Bou
753 Azzer ophiolite, Anti-Atlas, Morocco). Precamb. Res. 300, 151-167

754 Hodel, F., Triantafyllou, A., Berger, J., et al., 2020. The Moroccan Anti-Atlas ophiolites:
755 Timing and melting processes in an intra-oceanic arc-back-arc environment, Gondwana
756 Res. 86, 182-202

757 Ikenne, M., Souhassou, M., Saintilan, N.J., Karfal, A., El Hassani, A., Moundi, Y., Ousbih,
758 M., Ezzghoudi, M., Zouhir, M., Maacha, L., 2020. Cobalt-Nickel-Copper arsenide,
759 sulpharsenide and sulphide mineralisation in the Bou Azzer window, Anti-Atlas,
760 Morocco: One century of multi-disciplinary and geological investigations, mineral
761 exploration and mining. Geological Society, London, Special Publications, 502,
762 https://doi.org/10.1144/SP502-2019-132

763 Inglis, J.D., Samson, S., D'Lemos, R.S., Admou, H., 2003. Timing of regional greenschist
764 facies deformation in the Bou Azzer Inlier, Anti-Atlas: U–Pb constraints from syn-
765 tectonic intrusions. First meeting of IGCP 485, El Jadida, Morocco, 40–42pp.

766 Inglis, J.D., MacLean, J.S., Samson, S.D., D'Lemos, R.S., Admou, H., Hefferan, K., 2004. A
767 precise U– Pb zircon age for the Bleida granodiorite, Anti-Atlas, Morocco: implications

768 for the timing of deformation and terrane assembly in the eastern Anti-Atlas. J. Afr.
769 Earth Sc, 39, 277–283.

770 Lasobras, E., 2012. Composición mineral y relaciones de fase de los arseniuros de Co-Fe-Ni
771 del yacimiento de Aït-Ahmane (Bou-Azzer, Marruecos). Diferencias con otros
772 depósitos. TFM., Universidad de Zaragoza. Spain, 53p.

773 Leblanc, M., 1975. Ophiolites précambriennes et gîtes arséniés de Cobalt (Bon Azzer.
774 Maroc). PhD thesis, Univ. Paris VI, France, 329p.

775 Leblanc, M., 1981. Ophiolites précambriennes et gîtes arséniés de cobalt (Bou Azzer-Maroc).
776 Notes et mém. Serv. Géol. Maroc, 280, 311p.

777 Leblanc, M., Billaud, P., 1982. Cobalt arsenide orebodies related to an Upper Proterozoic
778 ophiolite: Bou Azzer (Morocco). Econ Geol. 77, 162-175.

779 Leblanc, M., Fischer, W., 1990. Gold and platinum group elements in cobalt-arsenide ores:
780 Hydrothermal concentration from a serpentinite source-rock (Bou Azzer, Morocco).
781 Miner. Petrol., 42, 197-209.

782 Levresse, G., 2001. Contribution à l'établissement d'un modèle génétique des gisements
783 d'Imiter (Ag-Hg), Bou Madine (Pb-Zn-Cu-Ag-Au) et Bou Azzer (Co-Ni-As-Ag-Au)
784 dans l'Anti-Atlas marocain. Ph.D. thesis, CRPG-CNRS, Nancy, France, 191p.

785 Lyubetskaya, T., Korenag, J., 2007. Chemical composition of Earth's primitive mantle and its
786 variance. J. Geophys. Res., 112, B03211. 21p

787 Maacha, L., 2013. Etude méallogéniques et géophysiques des minéralisations cobaltifères et
788 cuprifères de Bou-Azzer El Graara Anti Atlas Maroc (Tome 1). PhD thesis, Cadi Ayyad
789 University, Marrakech, Morocco, 344p.

790 Maacha, L., En-Naciri, O., El Ghorfi, M., Saquaque, A., Alansari, A., Soulaimani, A., 2011.
791 Le district à cobalt, nickel et arsenic de Bou Azzer (Anti-Atlas central). Notes et mém.
792 Serv. Géol. Maroc, 9, 91-97.

793 Maacha, L., Lebedev, V.I., Saddiqi, O., Zouhair, M., El Ghorfi, M., Borissenko, A.S.,
794 Pavlova, G.G., 2015a. Arsenide deposits of the Bou Azzer ore district (anti-atlas
795 metallogenic province) and their economic outlook. editor acad. RAS, doctor of
796 geology V.V. Yarmolyuk – Kyzyl: TuvIENR SB RAS, 66 p.

Maacha, L., El Ghorfi, M., En-Naciri, A., Sadiqqi, O., Soulaimani, A., Alansari, A., Bhilisse, M., 2015b. Nouvelles données isotopiques et d'inclusions fluides des minéralisations cobaltifères de Bou Azzer. Apport à la géologie économique de la boutonnière. (Anti-Atlas central, Maroc). Notes et mém. Serv. Géol. Maroc, 579, 133-139.

Marchesi, C., Garrido, C. J., Proenza, J.A., Hidas, K., Varas-Reus, M. I., Butjosa, L., Lewis J.F., 2016. Geochemical record of subduction initiation in the sub-arc mantle: Insights from the Loma Caribe peridotite (Dominican Republic). Lithos 252–253, 1–15.

Mrini, Z., 1993. Chronologie (Rb–Sr, U–Pb), traçage isotopique (Sr–Nd-Pb) des sources des roches Magmatiques éburnéennes, panafricaines et hercyniennes du Maroc PhD thesis, Cadi Ayad University, Marrakech, 227p.

Naïdoo, D.D., Bloomer, S.H., Saquaque, A., Hefferan, K., 1991. Geochemistry and significance of metavolcanic rocks from the Bou-Azzer-El Graara ophiolite (Morocco). Precamb. Res. 53, 79-97.

Naldrett, A.J., Duke, J.M., 1980. Platinum metals in magmatic sulfide ores. Science, 208, 1417-1424

Nataf, F., 2003. Jean epinat. Un homme, une aventure au Maroc. Souffles, 160 pp.

Oberthür, T., Melcher, F., Henjes-Kunst, F., Gerdes, A., Stein, H., Zimmerman, A., El Ghorfi, M., 2009. Hercynian age of the cobalt-nickel-arsenide-(gold) ores, Bou Azzer, Anti-Atlas, Morocco : Re-Os, Sm-Nd, and U-Pb age determinations. Econ Geol. 104, 1065–1079.

Oze, C., Bird, D.K., Fendorf, S., 2007. Genesis of hexavalent chromium from natural sources in soil and groundwater. PNAS, 104, 16, 6544 – 6549.

Pasava, J., 1994. Geochemistry and role of anoxic sediments in the origin of the Imiter silver deposit in Morocco. Czech Geol. Surv. Bull., 69, 1-11.

Samson, S.D., Inglis, J.D., D'Lemos, R.S., Admou, H., Blichert-Toft, J., Hefferan, K. 2004. Geochronological, geochemical, and Nd-Hf isotopic constraints on the origin of Neoproterozoic plagiogranites in the Tasriwine ophiolite, Anti-Atlas orogen, Morocco. Precamb. Res. 135, 133–147.

Saquaque, A., 1992. Un exemple de suture-arc de Précambrien de l'Anti-Atlas Centro-Oriental (Maroc). PhD thesis, Cadi Ayyad University, Marrakech, Morocco, 338.

Saquaque, A., Admou, H., Karson, J.A., Hefferan, K., & Reuber, I., 1989. Precambrian accretionary tectonics in the Bou Azzer-El Graara region. Geology, 17, 1107–1110.

Talha, M., 2011. Cartographie et métallogénie de la minéralisation arséniée à Co-Ni du filon 52, secteur d'Aït Ahmane, ophiolite de Bou Azzer, Anti-Atlas central, Maroc. Master, Cadi Ayyad University, Marrakech, Morocco, 91p.

Tekiout, B., 1991. Stratigraphie, pétrographie, géochimie et structure de l'ensemble arc/avant arc de la Boutonnière de Bou Azzer-El Graara (unité nord) Anti-Atlas Maroc. Thèse 3ème Cycle, Cadi Ayyad University, Marrakech, Morocco, 151p.

Triantafyllou, A., Berger, J., Baele, J.M., Mattielli, N., Ducea, M.N., Sterckx S., Samson S., Hodel, F., Ennih, N., 2020. Episodic magmatism during the growth of a Neoproterozoic oceanic arc (Anti-Atlas, Morocco). Precamb. Res. 339, April 2020, 105610

Ulrich, M., Munöz, M., Guillot, S., Cathelineau, M., Picard, C., Quesnel, B., Boulvais, P., Couteau, C., 2014. Dissolution–precipitation processes governing the carbonation and silicification of the serpentinite sole of the New Caledonia ophiolite. Contrib Mineral Petrol. 167: 952, 1-19.

## 9. Figure caption.

**Figure 1.** (A). simplified geological map of the Anti-Atlas belt. (B). Geological map of Bou Azzer inlier (Central Anti Atlas, Morocco) (modified from El Hadi et al., 2010), showing the main Co-Ni deposit in the district.

**Figure 2.** Geological map of Ait Ahmane area (modified from Saquaque, 1992), showing the position of Fe-Co ores.

Figure 3. Geological map of F55 and F56 lenses (Ait Ahmane area, Bou Azzer, Anti-Atlas); internal report of CTT mine Bou Azzer).

**Figure 4.** (a). Field observation of the main F55 lens in the Ait Ahmane district. (b to e). Microphotographs of rocks hosted F55 ores observed by LPA. (b). serpentinite rock composed mainly by serpentine (srp). (c & d). calcite (Cal) filling of irregular veinlets affecting serpentine (srp) and talc minerals (tlc). (e). fibrous texture of talc (tlc), containing scattered small magnetite crystals.

**Figure 5.** Microphotographs of ore minerals from F55 and F56 ores. (a). Chromite (Chr) replaced by löllingite (Lo). (b & c). löllingite rosettes (Lo) grains containing Co-Ni rich

diarsenides bands (Rm-Sf-Lo) and Bi inclusion (Bi); scattered in calcite in disseminated ores from F55 lens. (d & e). aggregates of spindle-shaped, zoned crystals of löllingite-safflorite included in calcite (F56 lens). (e) is zoom of (d) (f). map of chromite (Chr) altered into Fe-Cr-rich hydroxides (hdr); scattered in chlorite (Chl).

**Figure 6.** X-ray chemical distribution maps of Fe, Co, and Ni for two characteristic zoned löllingite rosettes from F55 ores (a. b. c) and F56 ores (d. e. f) (Ait Ahmane area, Bou Azzer district).

**Figure 7.** (a). Plot of diarsenides composition from F55 and F56 ores from Ait Ahmane area in the system $CoAs_2$–$NiAs_2$–$FeAs_2$. (b). Plot of skutterudite composition from F56 ores from Ait Ahmane area in the system $CoAs_3$–$NiAs_3$–$FeAs_3$. The compositional fields of di- and tri-arsenides analyzed by others authors from ores of the Ait Ahmane Area (Bou Azzer district; (En-Naciri, 995; El Ghorfi, 2006; Lasobras, 2012)) are also shown for comparison.

**Figure 8.** Compositional variations in terms of Cr–Fe3+–Al of accessory chromite grains associated to Fe-arsenide ores in F55 lens from Ait Ahmane area. The composition of chromite analyzed by others authors from Bou Azzer (peridotite mantle: Ahmed et al., (2005), serpentinite from Ait Ahmane area: Hodel et al., (2017); Ait Ahmane ores hosted in serpentinite: Fanlo et al., (2015); F7/5 deposit: Ares, (2018)) are also shown for comparison.

**Figure 9.** Primitive mantle-normalized As-Co-Ni-Fe spidergrams of ores from Ait Ahmane area (F56, F55 ores, and its host rocks), F7/5 and Aghbar deposits (Bou Azzer district, Morocco). Normalizing values are taken from Lyubetskaya and Korenaga, (2007).

**Figure 10**. As-Co, As-Ni, and As-Fe diagrams of ores from Ait Ahmane area (F55 and F56), F7/5 and Aghbar deposits (Bou Azzer district, Morocco).

**Figure 11.** Chondrite-normalized PGE spidergrams of ores from Ait Ahmane area (F56, F55 ores, and its host rocks), F7/5 and Aghbar deposit (Bou Azzer district, Morocco). Normalizing values are taken from Naldrett and Duke (1980).

**Figure 11.** Schematic bloc diagram of ores zoning in the serpentinite hosted ores (F55 lens, A), and in contact-type ores (B).

10. Table

**Table 1.** Whole-rock major ore-forming elements and noble metal contents.

887 Serpentinite-hosted, Fe-arsenide ores in the Ait Ahmane area in the easternmost part of the

888 Bou Azzer mining district.

889 New ore type showing zoning evolving from massive arsenide ores in core to arsenide-poor,

890 carbonated serpentinite halo.

891 Formation of Co-Fe and Fe arsenide ores by dissolution/precipitation of serpentinites

892 Bou Azzer district, central Anti-Atlas, Morocco

893

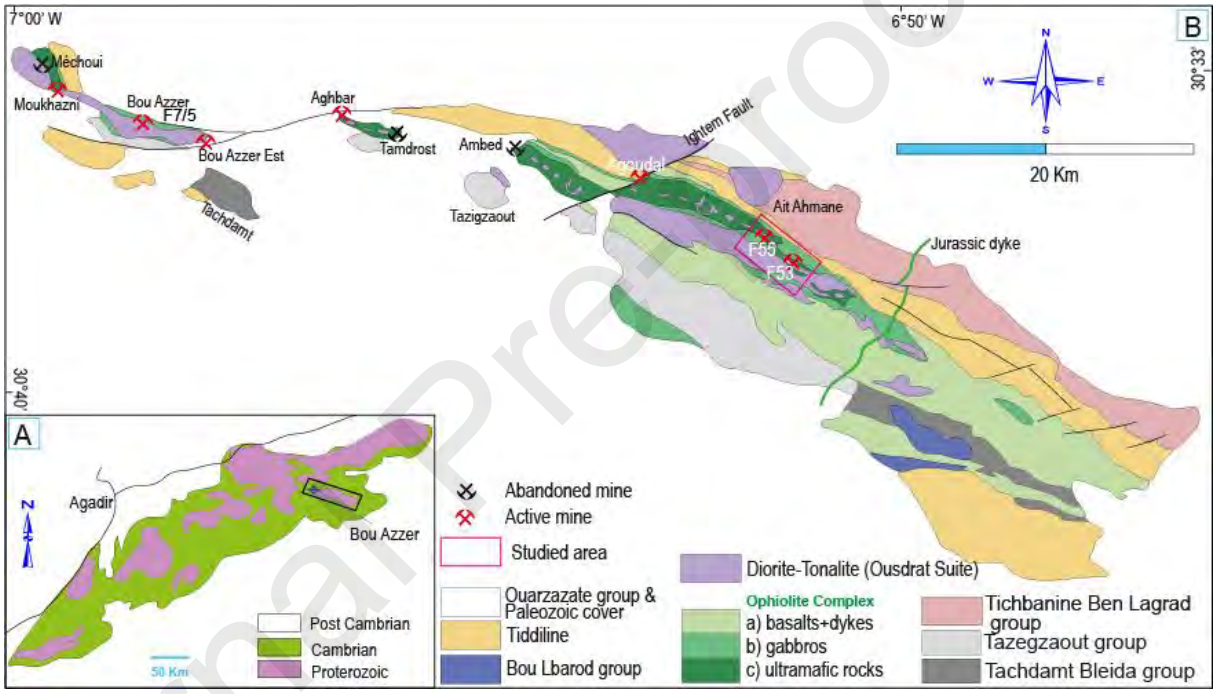


894

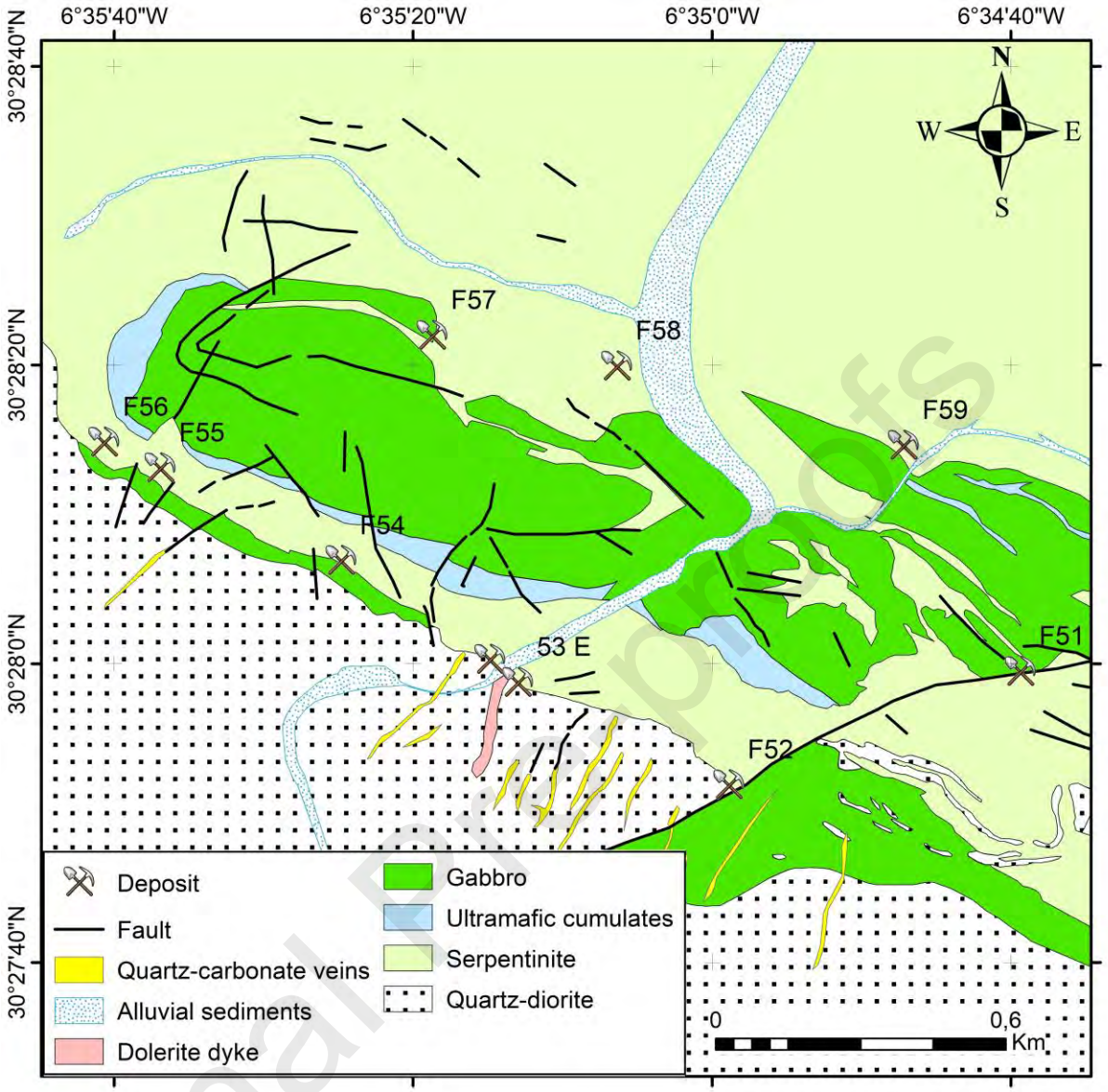


895

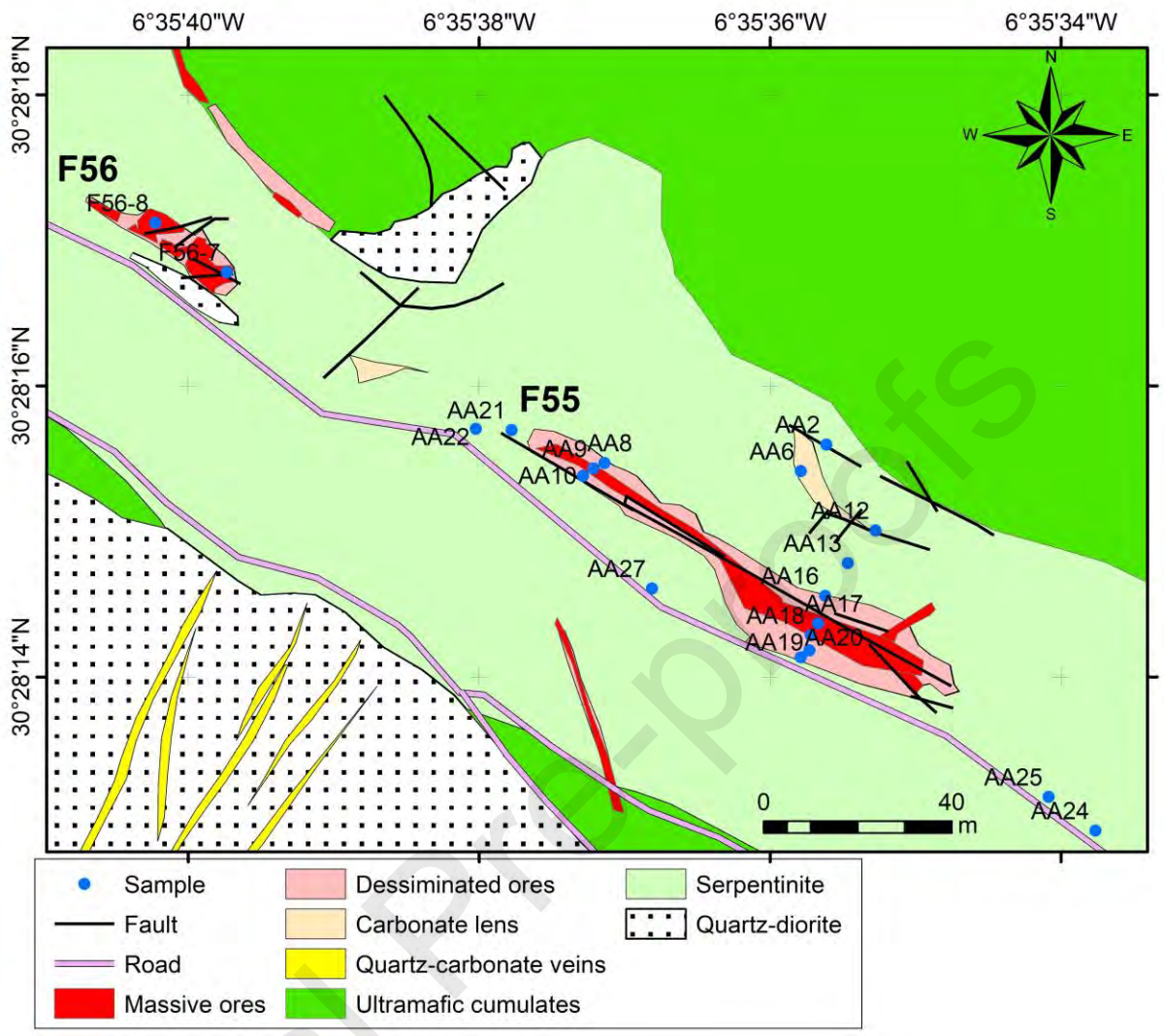


896

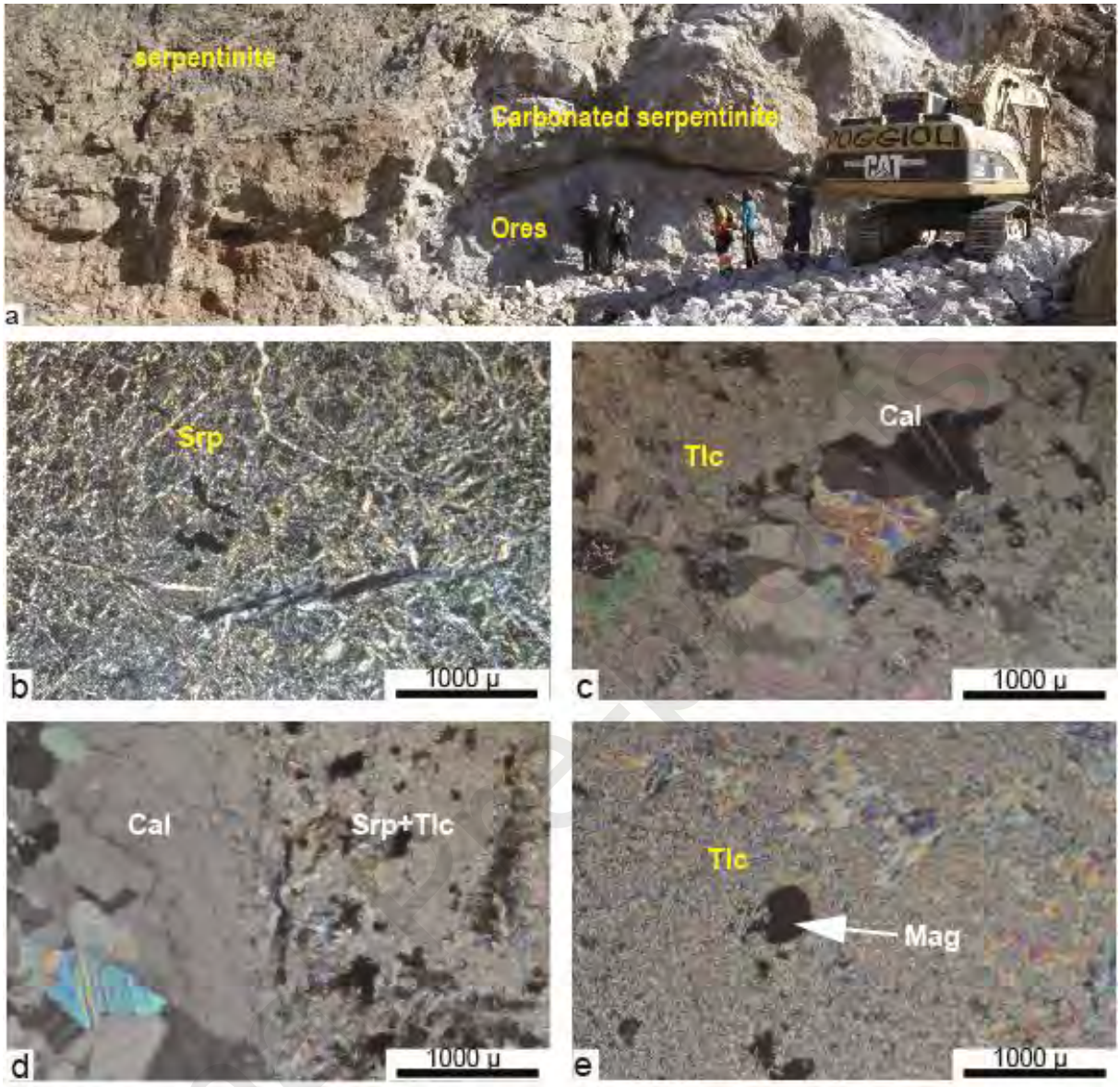


897

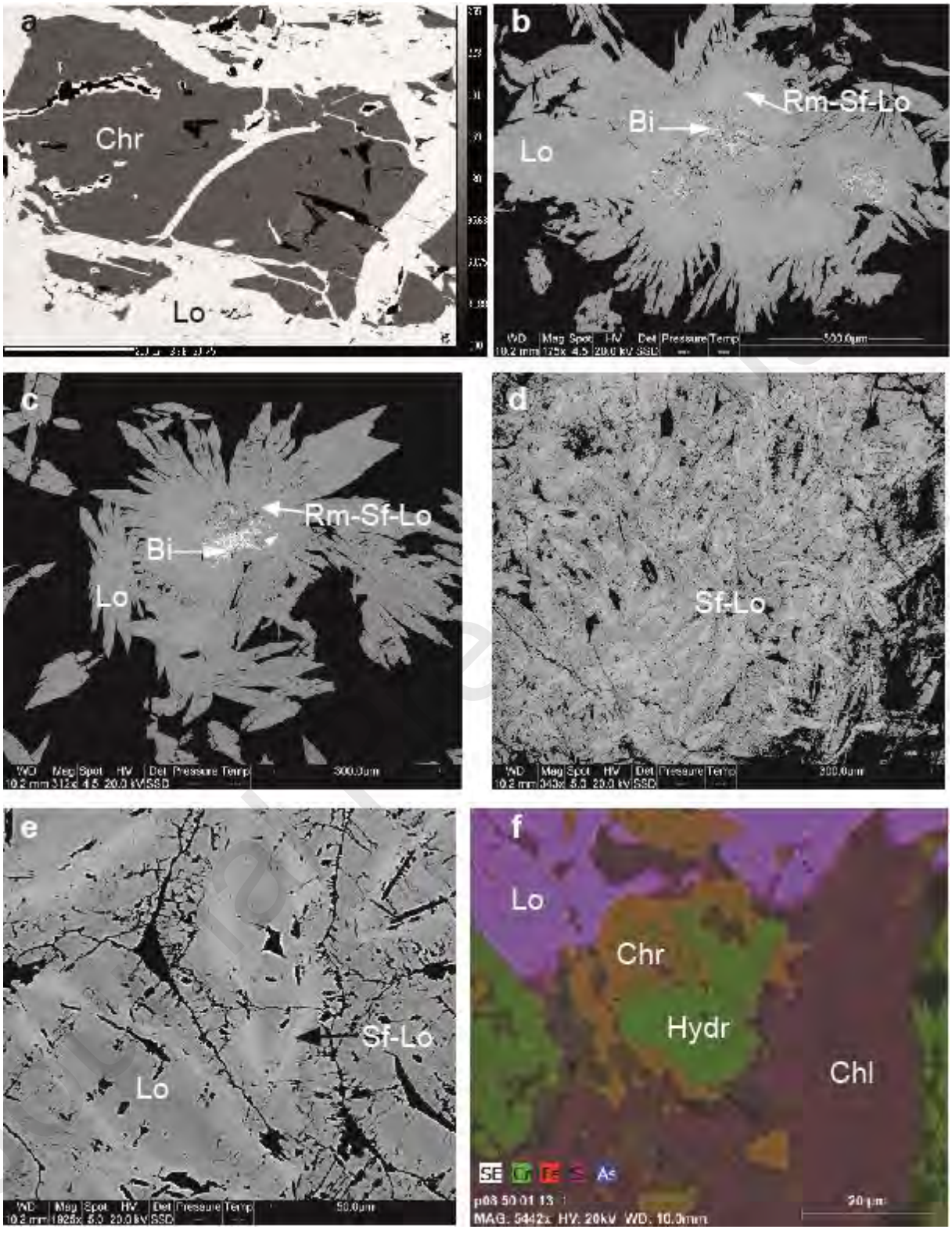
a
Chr
Lo
b
Bi
Rm-Sf-Lo
Lo
c
Rm-Sf-Lo
Bi
Lo
d
Sf-Lo
e
Sf-Lo
Lo
f
Lo
Chr
Hydr
Chl

898

899

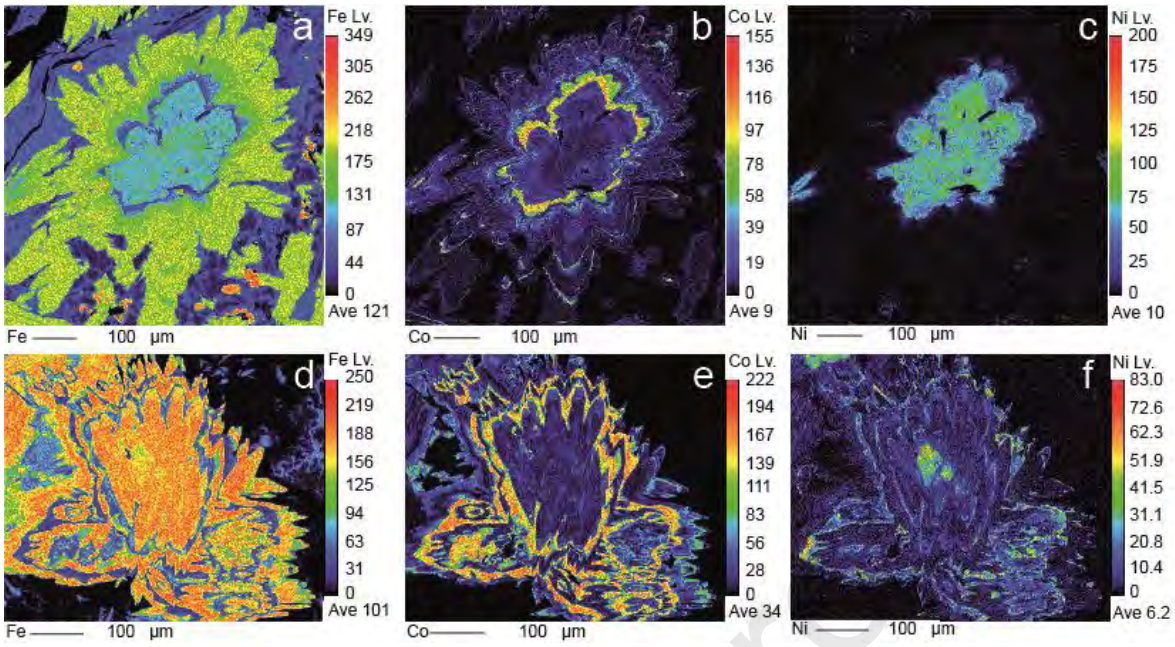


900

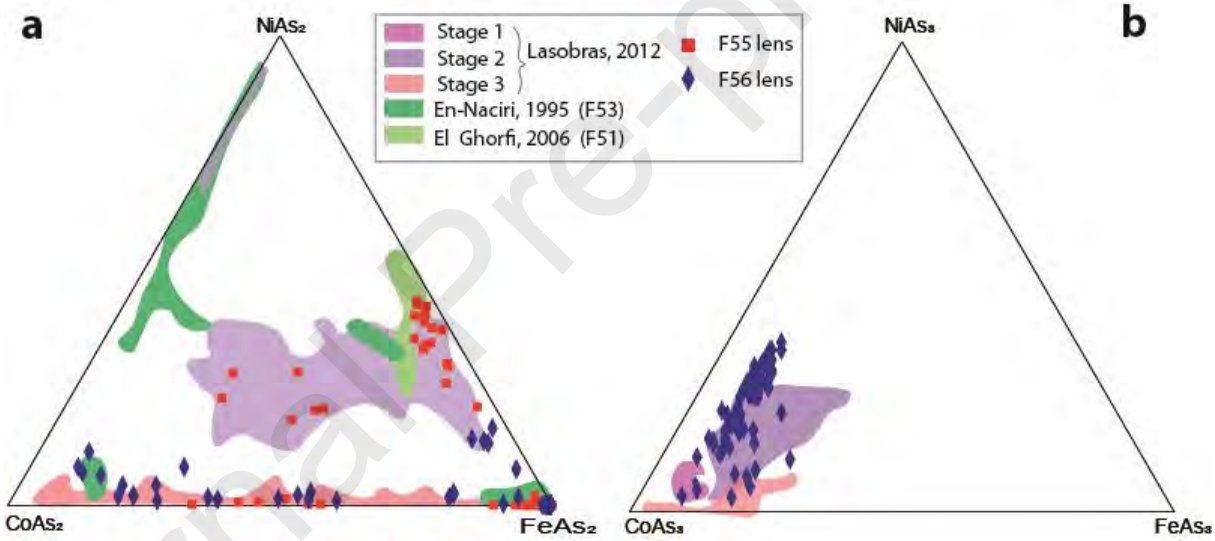


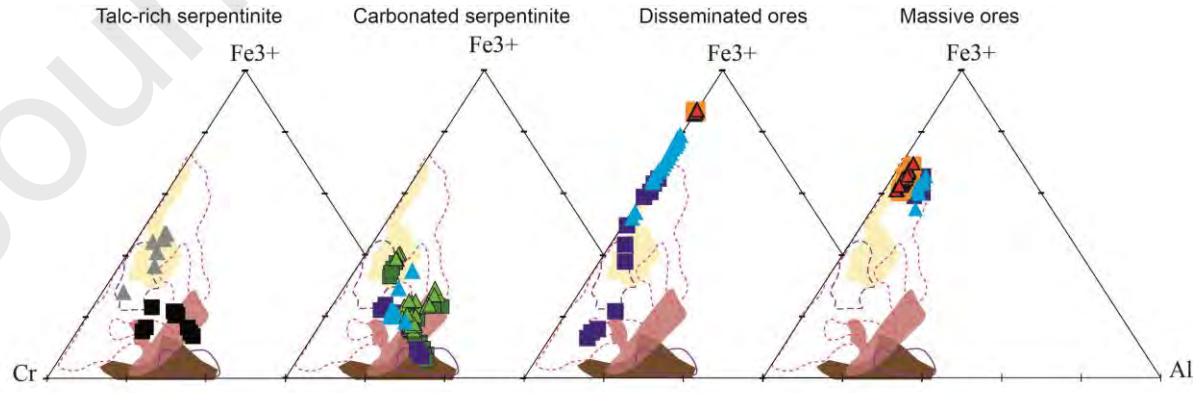


901

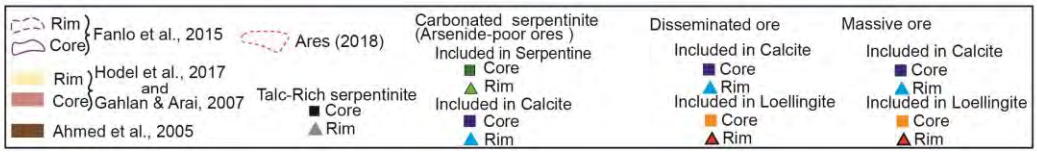



38

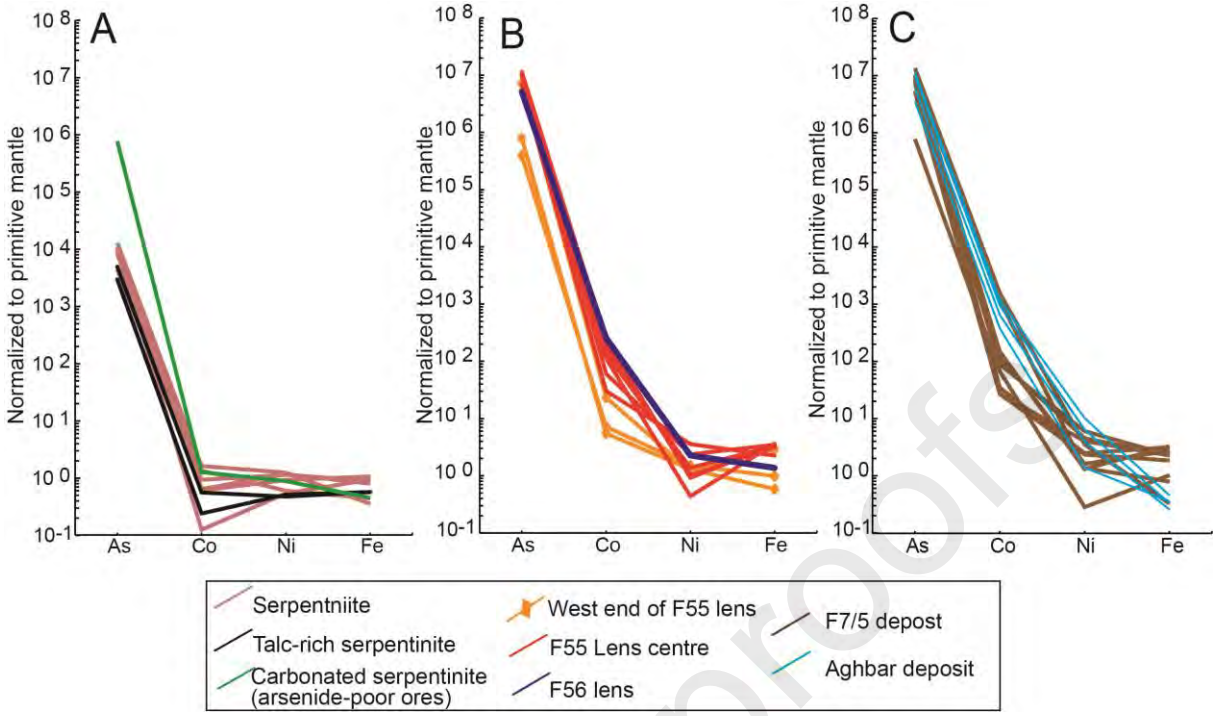


902

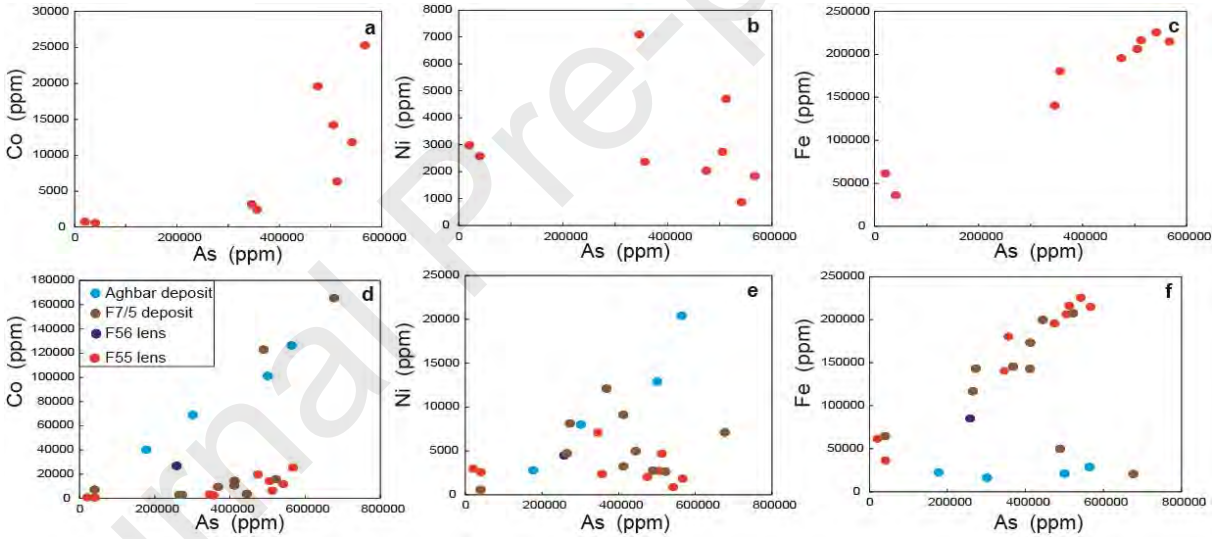


903




39

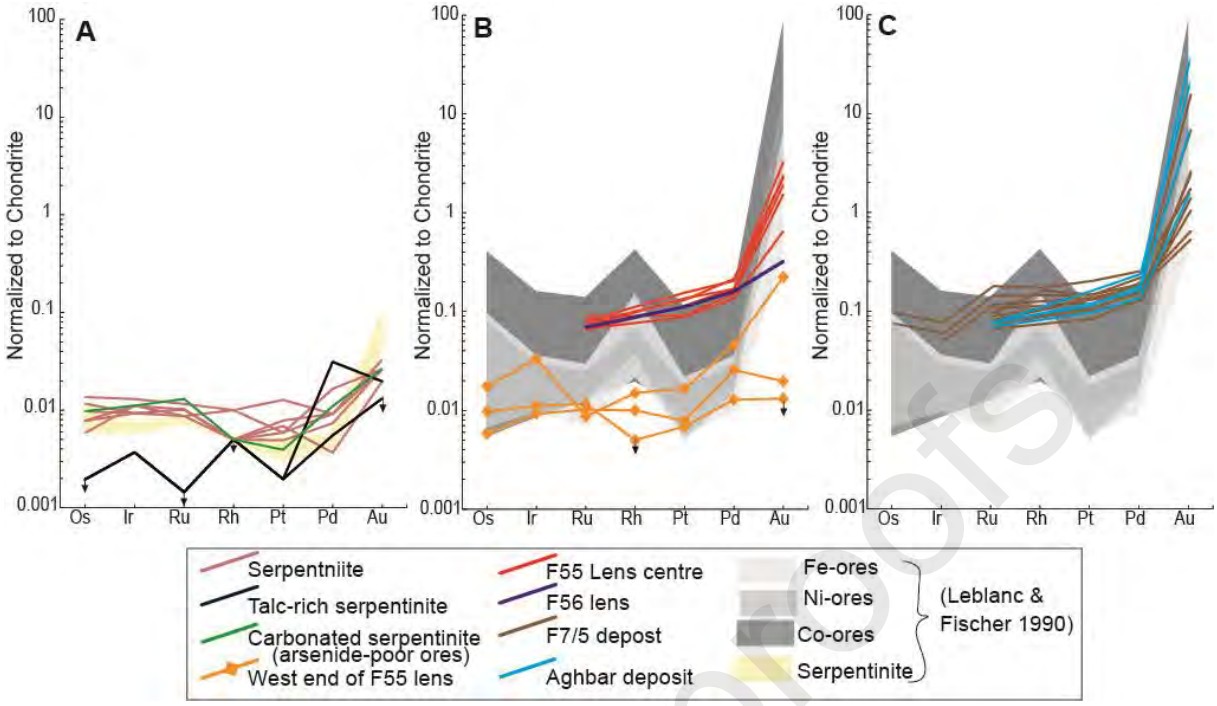
A
B
C
Normalized to Chondrite
100
10
1
0.1
0.01
0.001
Os
Ir
Ru
Rh
Pt
Pd
Au
Serpentniite
Talc-rich serpentinite
Carbonated serpentinite (arsenide-poor ores)
West end of F55 lens
F55 Lens centre
F56 lens
F7/5 depost
Aghbar deposit
Fe-ores
Ni-ores
Co-ores
Serpentinite
(Leblanc & Fischer 1990)

904

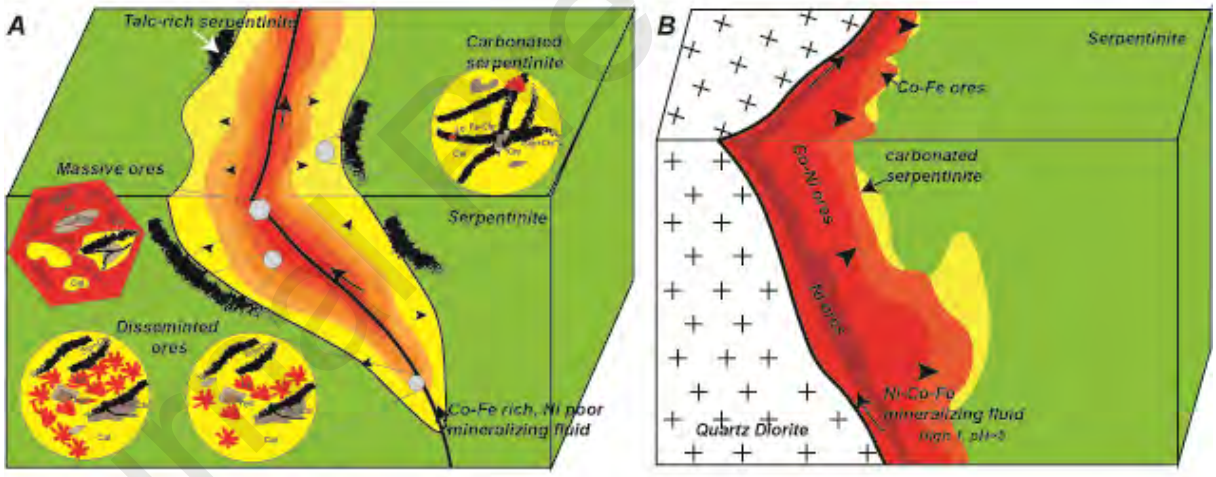
A
Talc-rich serpentinite
Carbonated serpentinite
Massive ores
Serpentinite
Disseminted ores
Co-Fe rich, Ni poor mineralizing fluid
B
Serpentinite
Co-Fe ores
carbonated serpentinite
Co-Ni ores
Fe ores
Quartz Diorite
Ni-Co-Fe mineralizing fluid

905


40

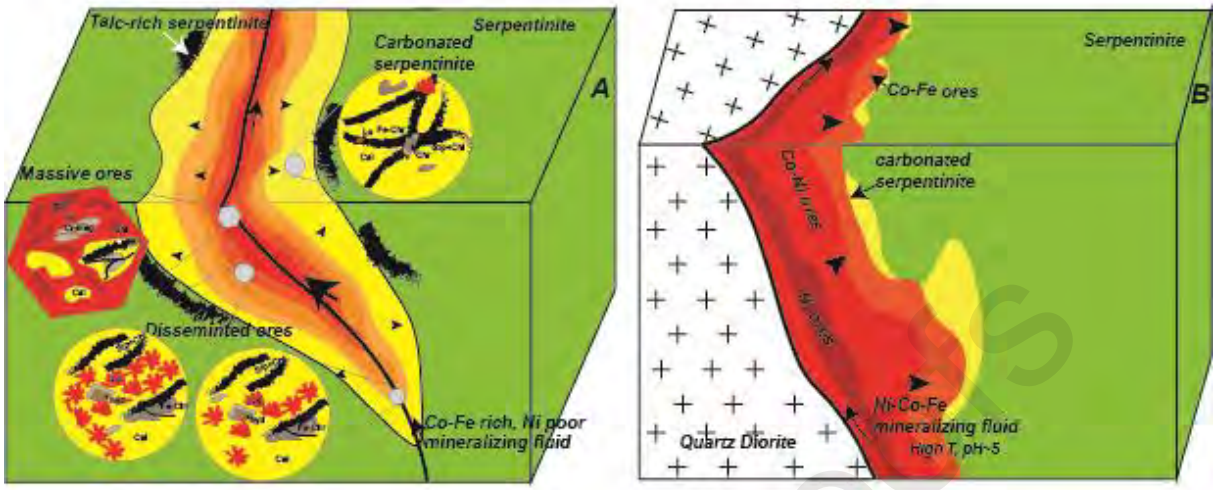


906